Review

Bianhong Li, Shaofeng Wu, and Xiangsheng Gao*

Theoretical calculation of a TiO_2-based photocatalyst in the field of water splitting: A review

https://doi.org/10.1515/ntrev-2020-0085
received September 16, 2020; accepted October 4, 2020

Abstract: Currently, energy and environmental problems are becoming more serious. The use of solar energy to split water and produce clean, renewable hydrogen as an energy source is a feasible and effective approach to solve these problems. As the most promising semiconductor material for photocatalytic water splitting, TiO_2-based nanomaterials have received increasing attention from researchers in academia and industry in recent years. This review describes the research progress in the theoretical calculations of TiO_2-based photocatalysts in water splitting. First, it briefly introduces some commonly used theoretical calculation methods, the crystal structure of TiO_2 and its photocatalytic mechanism, and the principle of doping and heterojunction modification to improve the photocatalytic performance of TiO_2. Subsequently, the adsorption state of water molecules with different coverages on the surface of TiO_2, the rate-limiting steps of the splitting of water molecules on the surface of TiO_2, and the transfer process of photogenerated current carriers at the interface between water molecules and TiO_2 are analyzed. In addition, a brief review of research into the theoretical calculations of TiO_2-based commercial photocatalysts in the field of water splitting is also provided. Finally, the calculation of TiO_2-based photocatalytic water-splitting simulations is summarized, and possible future research and development directions are discussed.

Keywords: theoretical calculation, water splitting, photocatalytic, TiO_2

*** Corresponding author: Xiangsheng Gao,** Beijing Key Laboratory of Advanced Manufacturing Technology, Faculty of Materials and Manufacturing, Beijing University of Technology, Chaoyang District, Beijing, 100124, China, e-mail: gaoxsh@bjut.edu.cn
Bianhong Li: School of Mechatronical Engineering, Beijing Institute of Technology, Haidian District, Beijing, 100081, China
Shaofeng Wu: Key Laboratory of Advanced Manufacturing Technology, Beijing University of Technology, Haidian District, Beijing, 100081, China

1 Introduction

The energy crisis is one of the two major problems facing the world today, and the development and utilization of new energy sources represented by solar energy and hydrogen energy are imminent. Since Fujishima and Honda [1] reported the production of hydrogen from the photocatalytic water splitting of TiO_2 in 1972, with high catalytic activity, good stability, nontoxicity to the human body, and low cost [2], it has become one of the most extensively studied and applied semiconductor materials in the field of photocatalysis [3].

Although the electron–hole pair generated by photoexcitation of TiO_2 possesses a strong redox ability as a result of the wide band gap (E_g = 3.0–3.2 eV), it does not effectively absorb visible light [4]. According to numerous experiments and theoretical calculations (Liu T. et al., December 2019, China United Test & Evaluation Qingdao CN110568122-A), the doping or heterojunction modification of TiO_2 not only effectively broadens its light absorption range but also substantially reduces the probability of photogenerated electron–hole pair recombination [5–14]. However, due to the complexity of the photocatalytic water-splitting reaction system, considerable controversy still exists regarding its reaction mechanism, reaction process, and kinetic behavior. Importantly, studies of the interaction between the surface of TiO_2 and water molecules, the energy barrier and rate-limiting steps of photocatalytic reactions, and the process of charge transfer are important methods to understand the mechanism of photocatalytic reactions. At the same time, this research also provides an important theoretical basis for improving the efficiency of hydrogen production from water splitting and improving the design of TiO_2-based photocatalysts [15,16].

With the rapid development of modern computer technology, molecular simulation has become a very important method and tool in many fields. Specifically, the methods of molecular simulation are generally divided

into the following categories: quantum mechanics methods [17], molecular mechanics methods [18], classical molecular dynamics [19], and molecular Monte Carlo methods [20]. The most widely used density functional theory (DFT) approach [21–25] was developed based on quantum mechanics methods (Guo S. et al., March 2019, Univ North Minzu CN109545286-A). The molecular mechanics method mainly relies on a molecular force field to calculate the various properties of the molecule, and its advantage is that it quickly obtains the various properties of the molecule. It is often used to analyze drugs, clusters, and biochemical macromolecules [26–28]. The molecular Monte Carlo method is based on the random movement of the particles in the system. It is the earliest nonquantum calculation method used for large systems, but this method is not suitable for the movement principles in physics. Compared with the molecular Monte Carlo method, the movement of system particles has the correct physical basis, and the calculation accuracy is high in classical molecular dynamics simulations. Meanwhile, the dynamic and thermodynamic statistics of the system are obtained, which are widely applicable to the discussion of various systems and characteristics. Currently, the theoretical calculation methods used to study photocatalytic water splitting of TiO_2 mainly include DFT based on quantum mechanics, classical molecular dynamics, and first-principles molecular dynamics combining DFT and classical molecular dynamics [29–31].

In addition to theoretical calculations of the structure of TiO_2 itself and the doped or heterojunction system [32–38], scholars have also conducted numerous theoretical calculations and experiments to determine the interaction between the TiO_2 surface and water molecules, the migration mechanism of photoproduced electron–hole pairs, recombination of electron–hole pairs and other steps in the process to obtain an understanding of the mechanism and essential laws of photocatalytic water splitting [39–46].

This review describes the research progress in theoretical calculations on the application of TiO_2-based photocatalysts in water splitting. First, it briefly introduces some commonly used theoretical calculation methods, the crystal structure of TiO_2 and its photocatalytic mechanism, and the principle of doping and heterojunction modification to improve the photocatalytic performance of TiO_2. Subsequently, the results of simulations and calculations of the adsorption and distribution structure of water molecules with different levels of coverage on the surface of TiO_2 are summarized. Then, the progress in simulations and calculations related to the rate-limiting steps of the water molecule splitting reaction on the surface of TiO_2 and the progress in the simulations and calculations of the photogenerated current carrier transfer process occurring at the interface of water molecules and TiO_2 are reviewed. In addition, a brief review of studies performing theoretical calculations of TiO_2-based commercial photocatalysts in the field of water splitting is also provided. Finally, the simulation and calculation of TiO_2-based photocatalytic water splitting are summarized, and possible future research and development directions are discussed.

2 Theoretical method

2.1 The first-principles calculation

The first-principles method is based on the principle of interactions between the nucleus and electrons and its law of motion, combined with the basic principles of quantum mechanics through some approximate processing steps to solve Schrodinger's equation. The generalized first principles include *ab initio* calculations based on density functional and *ab initio* calculations based on the Hartree–Fock self-consistent calculation. The former uses electron density as the basic variable, and by solving the Kohn–Sham equation, the ground state electron density of the system is procured iteratively and self-consistently to solve the ground state properties of the system. The latter obtains the wave function of the system by self-consistently solving the Hartree–Fock equation. Two basic approximations are included in the first-principles calculation method for solving the ground state properties, namely, the Bonn–Oppenheimer approximation [47,48] and single-electron approximation [49,50]. These two approximations are the key to solving multiparticle systems.

2.2 DFT

DFT originated from the electron density functional of kinetic energy based on the uniform electron gas model proposed by Thomas and Fermi in 1927, also known as the Thomas–Fermi model [51,52]. Subsequently, the Hohenberg–Kohn theorem and Kohn–Sham theorem were proposed based on this model, and the DFT was truly developed.

DFT is a method to reduce a 3N dimensional problem to a density problem of a three-dimensional particle, which substantially reduces the number of calculations

in practical applications. This reduction makes DFT completely different from the classical electronic structure theory based on complex multielectron wave functions. Currently, this theory is already one of the most commonly used methods in the fields of condensed matter physics and computational chemistry, and its appearance has facilitated the development of materials physical chemistry and other fields.

2.3 Exchange–correlation functional

DFT holds that all quantities are theoretically accurate, and only the exchange–correlation functional uses approximate methods. The usual approximation methods include local density approximation (LDA) and generalized gradient approximation (GGA) (Liu B. et al., August 2018, Univ Shenyang Technology CN108387636-A).

2.3.1 LDA

LDA is a simple and effective approximation in which electrons have a uniform electron density behavior in a uniform field, and their exchange–correlation energy is accurately calculated using the quantum Monte Carlo algorithm. When the external potential field does not change drastically, the uniform electron gas density function is used instead of the nonuniform electron gas density function to calculate the exchange–correlation energy in the local area [53,54].

The LDA method was widely used in the early DFT calculations [55], but it still has certain errors when calculating the solutions to some problems. For example, the lattice constant is usually too small during the calculation leading to a larger adsorption energy and bulk modulus of the system. The calculated diffusion barrier is often too low. The calculated band gap of a semiconductor usually produces a deviation greater than 50%, and sometimes an effective band gap value is not able to be obtained.

2.3.2 GGA

In practical applications, the performance of most semiconductor materials will improve after the introduction of some intrinsic defects or doping of some impure atoms. Due to the introduction of defects and impure atoms, the electron density in these semiconductor materials will undergo abrupt changes; therefore, the LDA method based on the uniform electron gas model is no longer suitable.

The GGA is developed based on LDA, and it not only uses the electron density as a variable of the exchange–correlation functional but also considers the gradient of density ($\nabla\rho$), thus strengthening its nonlocal description of charge density [56,57] and improving the calculation accuracy. Commonly used schemes include PBE, PW91, and RPBE.

2.3.3 Hybrid functional and Hubbard + *U*

When calculating values for transition metal oxides, LDA and GGA tend to underestimate their band gap size, and the value obtained is generally 1.0–2.0 eV less than the experimental value [58]. This discrepancy is attributed to the calculation of the properties of the ground state of the system by the common LDA and GGA methods, which are unable to accurately describe the local and delocalized characteristics of electrons. The potential function based on the LDA and GGA methods must be modified to more accurately describe the electronic properties of materials. Currently, researchers often use hybrid functional (HF) or Hubbard + *U* methods to solve these problems [59,60].

The so-called HF adds other functionals to modify the traditional LDA or GGA functionals. Compared with the two types of functionals described above, HF provides a more accurate description of the ion potential and lattice constants of the system. Common HFs include B3LYP (for molecular systems), PBE0 (25% HF and 75% DFT functionals; for solid systems), and HSE (for solid systems). However, compared with traditional functionals, the use of HF often requires more computing resources, which has become an important factor limiting its application.

In addition to using HF calculations, the Hubbard + *U* method is a more commonly used calculation method. The *U* in LDA + *U* or GGA + *U* refers to the strong correlation repulsion energy of electrons with opposite spins in the Hubbard model. Since both the LDA and GGA methods use a single-electron approximation to address valence electrons, they usually ignore the strong correlation between these two electrons when they calculate a strong correlation system containing d and f state electrons. Generally, a *U* value must be added in the calculation process to modify this method, which is generally only applicable to the strong correlation system containing d and f state electrons. In the TiO_2 system, the *U* value generally ranges from 2.5 to 4.5 eV, and different *U* values will also affect the lattice constant of the system,

particularly the electronic peculiarities, and thus a unified U value is required in the calculation [58,61,62].

2.4 Transition state theory

The transition state theory developed in the 1830s states that the chemical reaction from reactant to product undergoes a high-energy transition state structure. During the reaction, partial chemical bonds of the reactant molecules break to form a transition state and then recombine to form a product. The energy of the transition state is higher than the reactants and products, the energy increases from the reactant to the transition state, and the energy decreases from the transition state to the product. The transition state is the saddle point on the potential energy surface of the reaction and is the highest point of energy connecting the reactant and the product. The transition state has high activity and an unstable structure, and its existence in the reaction is short. The transition state structure is difficult to obtain experimentally; fortunately, the transition state structure can be effectively simulated through theoretical calculations [63]. The synchronous transition method proposed by Halgren et al. [64] automatically generates a continuous path search and predicts the transition state structure between known reactants and products, including linear synchronous transition (LST) and secondary synchronous transition (QST).

2.5 Molecular dynamics simulation

Molecular dynamics provide a definite microscopic description of a physical system, either a few-body system or a multibody system. The basic principle of this method is to establish a particle system, simulate the microscopic phenomenon under study, and determine the interaction between the particles using quantum mechanics [65]. For many particle systems conforming to the laws of classical Newtonian mechanics, the motion law and trajectory of the particle in the phase space are obtained from the numerical solution of the particle kinematics equation set, and then the corresponding macroscopic physical properties of the system are obtained according to the principles of statistical physics [66]. The motion equation of the particle is a set of ordinary differential equation sets, and the basic principle of the solution is to use the finite difference method to integrate the equation along the time axis with a certain time step. Although the accuracy of the molecular dynamics simulation is not as good as the first-principles simulation, its advantages, such as a convenient calculation process, small number of calculations, and high computable atomic system complexity, greatly exceed the latter and thus have broad development and application prospects [67].

In the process of a molecular dynamics simulation, the basic steps include determining the research object, establishing the potential energy model, establishing the corresponding molecular dynamics equation, initializing the configuration of the established microstructure, establishing the periodic boundary conditions of the computational model, and truncating the initial potential energy of the calculation model. The model of the target material system is simulated, calculated, and analyzed [68].

In the adhibition of molecular dynamics simulation methods, simulations are mainly conducted for the two types of system states. One is the simulation of the equilibrium state, and the other is the simulation of the non-equilibrium state. The main difference between the two systems is whether the amount of interest and the boundary conditions of the equilibrium system are related to time. A molecular dynamics simulation is always performed under a certain ensemble to accurately reflect the actual physical process [69].

3 Crystalline structure of TiO_2 and its photocatalytic mechanism

3.1 Crystalline structure of TiO_2

Three main crystal types of TiO_2 have been identified in nature, namely, brookite, rutile, and anatase [70]. Both rutile and anatase TiO_2 belong to the tetragonal system, while brookite TiO_2 belongs to the orthorhombic system. The structure of brookite TiO_2 is unstable, and its preparation is relatively difficult [71]; therefore, it is usually used for basic research. Meanwhile, rutile and anatase TiO_2 play a vital role in the field of photocatalysis applications.

Some similarities have been observed between the anatase and rutile crystal structures, namely, TiO_6 octahedrons constitute the most basic structure. However, at the same time, some differences also exist between the two crystal structures, including the degree of distortion and connection mode of the TiO_2 octahedron. The TiO_6 octahedron formed by rutile TiO_2 is closely connected

along the space c axis in the form of an edge sharing chain, and the octahedrons have a slight orthogonal distortion [72]. Compared with rutile TiO_2, the TiO_6 octahedron formed by anatase TiO_2 displays a more substantial orthorhombic distortion [73], and the symmetry is also poor. Regarding the connection mode, each octahedron in the rutile phase is coupled with 10 adjacent octahedrons, while in the anatase phase, each octahedron is coupled with 8 adjacent octahedrons. These differences in the lattice structure result in different mass densities and electronic band structures of the two forms of TiO_2 [74]. The mass density of anatase TiO_2 is 3.894 g/cm^2, which is slightly smaller than the value of 4.250 g/cm^2 for rutile.

According to recent studies, the photocatalytic property of rutile TiO_2 is slightly lower than anatase TiO_2 [75–77]. In fact, the energy gap (3.0 eV) of rutile phase TiO_2 is narrower than the anatase phase (3.2 eV), and the energy required for electrons to be excited to transition is relatively small; therefore, the light response range of rutile phase TiO_2 is wider. However, the rutile phase TiO_2 tends to have a larger particle size and form an agglomerated structure, leading to easy recombination of the electron–hole pairs [78]. Conversely, the anatase phase crystal lattice contains more defects and dislocations, which increase the separation of electron–hole pairs generated in this lattice, resulting in a stronger photocatalytic property of‘ anatase phase TiO_2 than the rutile phase.

3.2 Photocatalytic mechanism of TiO_2

As shown in Figure 1, based on the solid energy band theory, the energy band structure of semiconductor TiO_2 is very different from that of metals or insulators, as it contains a valence band (VB), a conduction band (CB), and a region between the CB and the VB called the band gap. The formula used to calculate the band gap (E_g) is $E_g = E_{VB} - E_{CB}$, where E_{CB} corresponds to the bottom potential of the CB, and E_{VB} corresponds to the top potential of the VB [79,80]. When the energy of the incident photon is equal to or greater than the E_g of TiO_2, the electrons in the VB will shift to the CB, and the holes will be generated in the VB, thus forming a photogenerated electron (e^-)–hole (h^+) pair [81,82]. Subsequently, under the action of an electric field, the formed electrons and holes will be separated, gradually transferred to the active sites on the surface of TiO_2, and react with the water molecules adsorbed on the surface of TiO_2 in the corresponding hydrogen evolution reaction (HER) or oxygen evolution reaction (OER) before finally decomposing the water molecules into H_2 and O_2 [83].

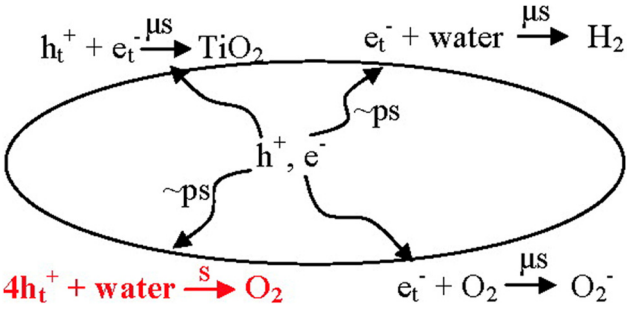

Figure 1: Schematic of the TiO_2 photocatalytic water-splitting mechanism, reprinted with permission from ref. [77], Copyright (2008) American Chemical Society.

The high overpotential in the OER will cause a substantial loss of energy, limiting the efficiency of photocatalytic reactions and practical applications. Therefore, the mechanism of OER must be elucidated to improve the photocatalytic efficiency, and it is a research hotspot in TiO_2 photocatalytic reactions. As shown in a previous study [84], the OER is a four-step reaction process, and every electron transfer reaction is accompanied by the loss of protons. The first step of the reaction is the reaction of photogenerated holes with water molecules or the reaction of holes with OH- and Ti-OH groups [85,86]. However, photoelectric emission spectroscopy data show that the O 2p energy level of water species is below the valence-band maximum (VBM) of TiO_2 [87], revealing the irrationality of the traditional four-step reaction mechanism from a thermodynamic perspective. Subsequently, through further experimental technical measurement and characterization, two new mechanisms, the redox photooxidation (RP) mechanism [88,89] and nucleophilic (NA) reaction mechanism [90,91], have been proposed in succession. In both of these mechanisms, the O atoms on the TiO_2 lattice are the active sites for trapping holes, and not the O atoms on the water molecules. However, significant differences have also been identified between these mechanism, mainly including the initial hole capture site, the role of water molecules in the reaction, and the source of oxygen. To date, the mechanisms of RP and NA have been extensively discussed and supported by some theoretical studies. However, most theoretical studies still adhere to the earlier mechanism, namely, the first step in the OER is to capture holes in the H_2O molecules on the TiO_2 surface. Researchers propose that the theory that the hole is initially localized in the protonated O_{br} in the RP mechanism is not accurate. Theoretically, this site is not the most advantageous hole capture site in the solution medium. Overall, a

consensus on the active site of hole capture has not been achieved, and further research and discussion are needed.

4 Doping modification of TiO_2

Doping refers to the method of replacing some atoms in TiO_2 with atoms of other elements, changing its band gap by changing its VB or CB edge. Common doping methods include nonmetal doping (Cai J. et al., November 2017, Jiangsu Haipu Functional Materials Co CN107376974-A), metal doping, and metal–nonmetal co-doping [92–95].

4.1 Non-metal doping

In 2001, Asahi et al. [96] prepared the $TiO_{2-x}N_x$ photocatalyst with nonmetallic element N-doped TiO_2 in a study conducted in Japan, resulting in a new field of visible light-mediated catalysis using nonmetallic-doped TiO_2. In the nitrogen-doped anatase TiO_2, the N 2p and O 2p hybrid orbital energies are very close, which reduces the band gap of N-TiO_2 and broadens the absorption range to visible light. The doping of TiO_2 with nonmetal elements is the main method to improve its photocatalytic performance, because the configuration of extranuclear electrons of non-metal elements is similar to the structure of oxygen atoms, with little effect on the original structure of TiO_2. Concretely, nonmetallic doping usually uses carbon, nitrogen and other atoms that contain more empty p orbitals than oxygen to replace the oxygen atoms in TiO_2, and thus the VB of TiO_2 is shifted upwards to reduce its band gap [97,98]. According to the first principles of DFT, Tian and Liu [99] calculated that S-doped anatase TiO_2 produces an S 3p hybrid energy level in the forbidden band and the VB shifts upward; thus, the band gap decreases, resulting in a redshift of the absorption spectrum. As the dopant concentration increases, the band gap is reduced and the redshift of the absorption spectrum is increased. As shown in Figure 2(a), Peng et al. [100] analyzed the effect of the P doping concentration on the absorption spectrum of anatase TiO_2 through theoretical research and found that the absorption spectrum exhibited a redshift as the doping concentration increased under low-concentration doping, but the absorption spectrum exhibited a blueshift as the doping concentration increased under high-concentration doping. In addition, the doping of non-metallic elements may also form isolated impurity energy levels above the VB, which will also broaden the light absorption range of TiO_2 [101].

4.2 Metal doping

Metal ions are effective electron acceptors. When doped with metal ions in TiO_2 crystals, the trapping of electrons in TiO_2 by the metal ions prolongs the recombination time of photogenerated electrons and holes in TiO_2 to improve the photocatalytic efficiency of TiO_2. In metal doping, transition metals such as Ni, Cu, Cr, Co, and Fe are usually used to replace titanium atoms [102,103]. If the CB of the doped metal is lower than titanium, the band gap of the doped TiO_2 will decrease [104]. Lian et al. [105] synthesized Mo-doped TiO_2 nanoparticles using the sol–gel method and observed that Mo^{6+} ions occupy the lattice position of anatase phase TiO_2 and reduce the band gap from 3.19 to 3.05 eV. The doping of Mo also increases the light absorption of TiO_2 in the ultraviolet and visible range, and the increase in ultraviolet light absorption is basically related to the charge transfer process of O^{2-} (2p) and Ti^{4+} (3d). The increase in visible light absorption results from electron transfer from the O 2P state to the Mo 4D state and the transition of the Mo 4D and Ti 3D states in the forbidden band (Figure 2(b) and (c)). Karvinen et al. [106] used the first-principles Hartree–Fock calculation method to establish a supercell system with atomic clusters and studied the electronic properties of a series of metal cations after doping into TiO_2. The doping of V^{3+}, Mn^{3+}, Cr^{3+}, and Fe^{3+} ions into the anatase phase TiO_2 shortens the band gap of the doped system, but V^{3+} and Fe^{3+} ions basically have no effect on the band gap size of the rutile phase TiO_2. In addition, the doped metal ions extend the range of light absorbed to the visible light region, ensuring that TiO_2 display a strong response to visible light. However, most of the doped metal ions are heavy metal ions, which will cause certain damage to the environment and limit its development and application.

4.3 Nonmetal–metal co-doping

Regardless of whether metal doping or nonmetal doping are used, a certain defect state likely occurs. Transition metal doping will produce an occupied interstitial state in the semiconductor forbidden band, and the charge of this interstitial state will be localized in doped metal atoms and may become exciton recombination centers and

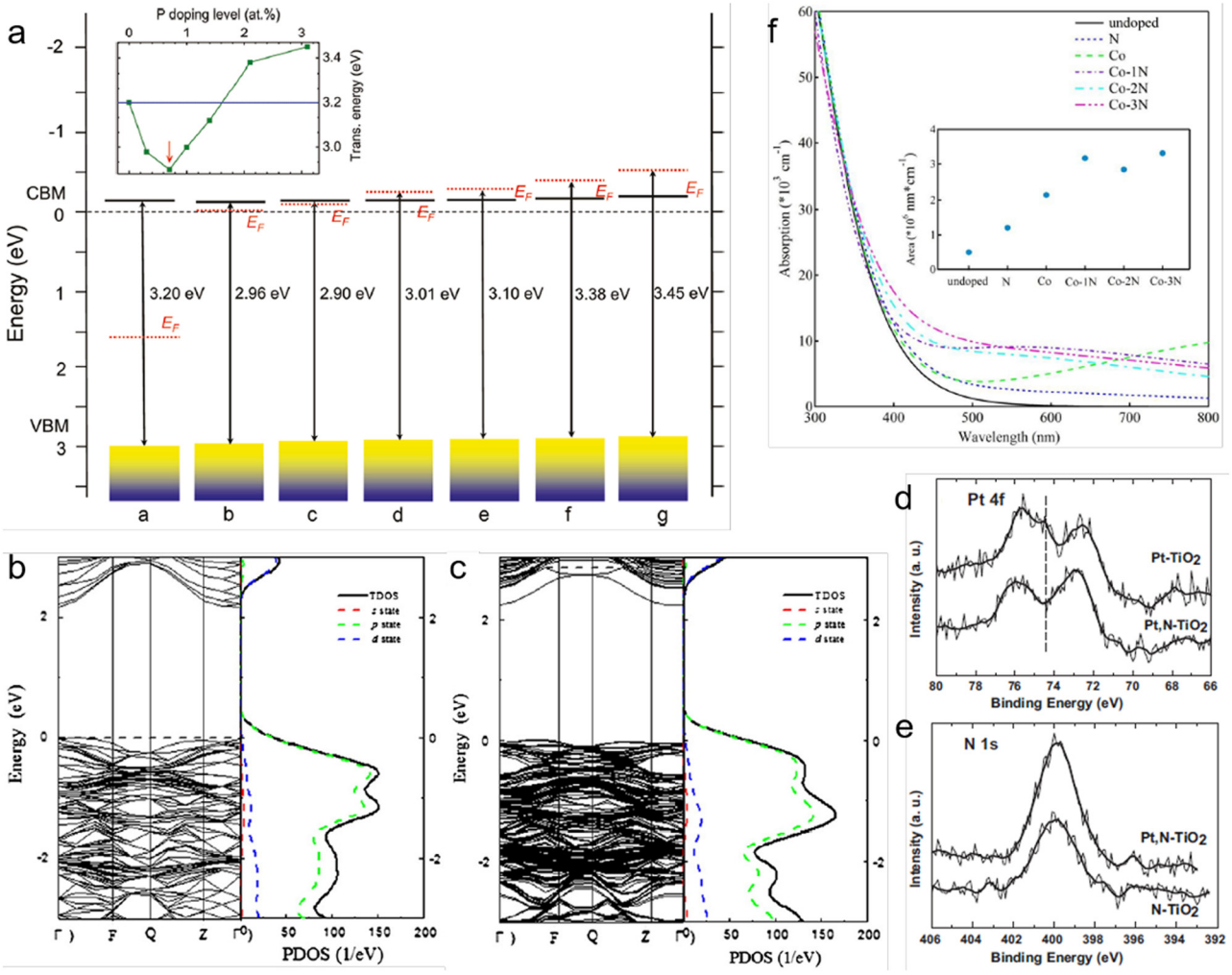

Figure 2: (a) Electron transition energy for the configurations of pure anatase and anatase with various P doping levels, reprinted with permission from ref. [98], Copyright (2011) American Chemical Society. Band structures of (b) TiO_2, and (c) $Ti_{0.98}Mo_{0.2}O_2$, reprinted with permission from ref. [103], Copyright (2013) Elsevier. XPS spectra of (d) Pt 4f and (e) N 1s levels in Pt-, N-, and Pt, N-TiO_2, reprinted with permission from ref. [108], Copyright (2014) Elsevier. (f) The optical absorption spectra of undoped, N-, Co-doped, Co-1N-, Co-2N, and Co-3N co-doped TiO_2, reprinted with permission from ref. [40], Copyright (2017) Elsevier.

cause a decrease in photocatalytic ability. Experiments have also confirmed this hypothesis. Nonmetallic doping of nitrogen and carbon is also believed to produce empty p orbitals in the band gap. This p orbital is also considered the recombination center of excitons. Notably, the co-doping of metals and nonmetals solves this problem. Using nitrogen–chromium co-doped TiO_2 as an example, the basic idea of this doping method is that chromium will produce occupied d orbitals and nitrogen will produce empty p orbitals. During co-doping, d electrons will enter the empty p orbitals, resulting in a full orbit of the VB and completely empty orbit of the CB, thereby avoiding the generation of exciton recombination centers [107]. At the same time, co-doping has been shown to shorten the band gap of TiO_2 by 1 eV [108].

Kim et al. [109] synthesized Pt/N co-doped TiO_2 using a wet chemical method. The specific surface area of Pt/N co-doped TiO_2 (178 m^2/g) is larger than undoped TiO_2 (110 m^2/g). A time-resolved diffuse reflectance spectroscopy (TDR) study of Pt/N-TiO_2, revealed a synergistic effect of co-doping. In addition, Pt ions only exist in the form of Pt^{4+} in Pt/N-TiO_2. As shown in Figure 2(d) and (e), the results of photoelectron spectroscopy (XPS) indicate an intervalence charge transfer transition. First-principles calculations also show that the electronic interaction of Pt and N in TiO_2 accelerates the mobility of current carriers, thereby improving the photocatalytic activity. Sun et al. [110] used a sol–gel method to prepare TiO_2 co-doped with Ce and N and found that Ce doping effectively inhibits the transformation of TiO_2 from the anatase

phase to the rutile phase. Moreover, He et al. [40] studied the properties of Co–N co-doped TiO_2 through first-principles calculations. Due to the reduction of the band gap and ILs between VB and CB, the light absorption limitation and the absorption scope of the Co-2N co-doped system increased significantly (Figure 2(f)).

5 TiO_2-based heterojunction

5.1 Metal/TiO_2

For the precious metal/TiO_2 prepared using the sol–gel method, the precious metal elements relatively easily enter the TiO_2 lattice to replace Ti ions. The appearance of this heterojunction extends the absorption band edge of TiO_2 to the visible region and even near infrared region. Generally, the doping of a small amount of precious metal produces impurity energy levels above the VB or below the CB of TiO_2. These impurity energy levels have been used as shallow acceptor levels or shallow donor levels and then become effective traps for photogenerated electrons. As shown in Figure 3(a), Yang et al. [111] used theoretical calculations based on DFT to study the photodeposition of Au or Ru precious metal clusters with excellent electronic properties as cocatalysts on the anatase phase TiO_2(101) surface and the mechanism of enhanced photocatalytic activity. As a result, the synthesized Ru/TiO_2 and Au/TiO_2 both showed excellent HER activity (Figure 3(b)). This significant increase in HER activity is due to the interfacial interaction of the catalyst, namely, the strong chemical bonds at the interface serve as electron traps for providing photoinduced electrons (Figure 3(c)). Due to the presence of Ru-4d and Au-5d electronic impurity states, the formation of new degenerate energy levels causes the band gap of the catalyst to

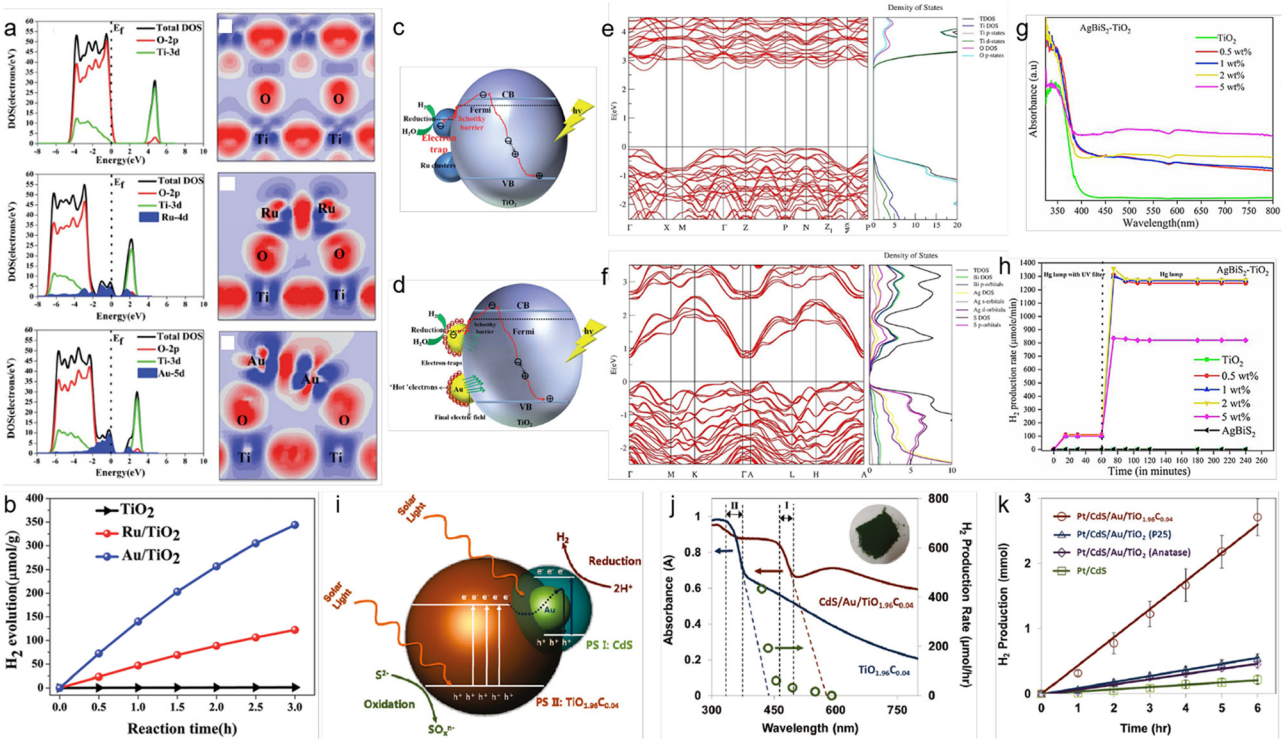

Figure 3: (a) Density of states and difference in the charge density of the configuration model of anatase TiO_2, Ru/TiO_2, and Au/TiO_2, respectively. (b) Photocatalytic H_2 evolution reactions mediated by various photocatalysts. (c) Schematic of the mechanism of electron-traps for photocatalytic overall water splitting. (d) Schematic of the mechanism of intensification of SPR, reprinted with permission from ref. [111], Copyright (2020) Royal Society of Chemistry. Calculated electronic structure and PDOS of (e) TiO_2 and (f) $AgBiS_2$, and (g) DRS spectra of TiO_2 and $AgBiS_2$–TiO_2 composites. (h) The H_2 production rate of the solution at varying weight percentages of $AgBiS_2$–TiO_2 catalysts, reprinted with permission from ref. [37], Copyright (2019) Elsevier. (i) CdS/Au/$TiO_{1.96}C_{0.04}$ was designed to mimic the natural photosynthesis system. (j) UV-vis absorbance spectrum of the CdS/Au/$TiO_{1.96}C_{0.04}$ powder and the effect of the light wavelength on H_2 evolution via water splitting on Pt/CdS/Au/$TiO_{1.96}C_{0.04}$. (k) H_2 production via photocatalytic water-splitting, reprinted with permission from ref. [120], Copyright (2011) American Chemical Society.

narrow. Moreover, the synthesized Au/TiO_2 exhibits a faster HER rate than Ru/TiO_2, which is attributed to the effect of surface plasmon resonance (SPR). As shown in Figure 3(d), a synergistic effect of plasma-induced "hot" electrons is observed that enhances the final built-in electric field harvest, promotes the migration and separation of photogenerated current carriers, and effectively increases the precipitation rate of hydrogen in the overall photocatalytic water-splitting reaction.

On the other hand, as a promising photocatalytic material for overall water splitting, TiO_2 effectively improves its low efficiency for HER by loading appropriate metal cocatalysts. Zhou et al. [12] used first-principles simulation calculations to deeply explore the working mechanism of a TiO_2 photocatalyst loaded with the non-noble metal Ni in the HER. Compared with the (001) crystal plane of TiO_2, Ni_n clusters more easily aggregate on the (101) crystal plane of TiO_2, and the structural difference between the two crystal planes determines this characteristic. The Ni_n clusters adsorbed on the surface of TiO_2 facilitate the separation of photogenerated current carriers and introduce the interstitial state into the forbidden band of TiO_2, which increases the Fermi level to a higher energy region, effectively improving the efficiency of the HER. Subsequently, electrochemical calculations were used to further study the process of hydrogen production by TiO_2. The active site of HER in the Ni_n/TiO_2 composite material is the O_{2c} atom that is bound to or close to the Ni_n cluster. Compared with clean surfaces, the loading of Ni_n clusters significantly reduces the Gibbs free energy of the HER. The authors reveal the growth behavior of the Ni cocatalyst on the surface of anatase TiO_2 and provide a reasonable explanation for the experimental improvement in the HER efficiency of TiO_2 after the introduction of Ni cocatalyst.

5.2 Semiconductor/TiO_2

5.2.1 Type II heterostructure

In the type II heterojunction, the positions of CB and VB of semiconductor A are all higher than semiconductor B. Based on the difference in the chemical potential between semiconductors A and B, the CB and VB at the interface of the type II heterojunction will be bent, and then a built-in electric field will be formed, enabling the spatial separation of photoexcited electrons and holes (Li H. et al., Univ Qingdao CN107096548-A). Considering the energy band structure of TiO_2, researchers usually choose narrow band gap semiconductors to combine with TiO_2 to form a type II heterojunction, such as CdS/TiO_2 [112], Cu_2O/TiO_2 [113], CeO_2/TiO_2 [114], Bi_2S_3/TiO_2 [115], MoS_2/TiO_2 [116], and other heterojunctions, which are all effective methods to increase the light response of TiO_2 to the visible region. In recent years, ternary narrow band gap semiconductors that match the solar spectrum are often selected to increase the absorbance coefficient of TiO_2 to a greater extent. For example, Pillai et al. [37] successfully synthesized a new type of heterojunction $AgBiS_2$–TiO_2 composite photocatalyst using a solvothermal method. Then, the electronic and optical capabilities of $AgBiS_2$ and TiO_2 were studied using DFT (Figure 3(e) and (f)). XRD results revealed tetragonal crystal forms of both $AgBiS_2$ and TiO_2. XPS and TEM results illustrate the formation of a heterostructure. As shown in Figure 3(g), due to the coupling between $AgBiS_2$ and TiO_2, the UV-DRS spectra of all composite photocatalysts show increased absorption of visible light. As the dopant concentration increases, the band gap of the composite photocatalyst also decreases. Upon exposure to visible light, the photocatalytic hydrogen production by the $AgBiS_2$/TiO_2 heterojunction is significantly increased, and the output is 1,000 times higher than pure TiO_2 (Figure 3(h)). As confirmed by the PL measurement, the reinforced photocatalytic efficiency is ascribed to the reduced recombination rate of photogenerated excitons. In addition, the author also performed free radical scavenging experiments and a theoretical analysis to define a reasonable photocatalytic mechanism.

5.2.2 Z-scheme heterostructure

The Z-scheme heterojunction is usually composed of a photocatalyst that produces H_2, a photocatalyst that produces O_2, and an electron mediator [117,118]. The main advantage of the Z-scheme heterojunction is that it combines the strongest reduction and oxidation capabilities of the two photocatalysts. Therefore, the Z-scheme heterojunction has been extensively used in water-splitting [119]. Yi et al. [120] reported the visible light-responsive Z-scheme heterojunction photocatalyst CdS/Au/$TiO_{1.96}C_{0.04}$. As shown in Figure 3(i), upon exposure to visible light, the photoinduced electrons on the surface of $TiO_{1.96}C_{0.04}$ are transferred to CdS through Au and recombined with the photoinduced holes on the CdS surface such that the CdS surface retains the photogenerated electrons with higher reducing power; at the same time, the $TiO_{1.96}C_{0.04}$ surface retains the photogenerated holes with higher oxidizing power. Using this approach, the CdS photocatalytic hydrogen production and $TiO_{1.96}C_{0.04}$ photocatalytic oxygen

production are effectively improved at the same time (Figure 3(j) and (k)). Yang et al. [121] constructed an 0D/1D g-C_3N_4/TiO_2 Z-scheme heterostructure containing an interfacial oxygen vacancy layer. The g-C_3N_4/TiO_2 photocatalyst shows the best photocurrent density at 1.23 V upon irradiation with light in the visible region (relative to the reversible hydrogen electrode), with a value as high as 0.72 mA/cm^2, which is 8 times higher than the sample without the interfacial oxygen vacancy layer. EIS also shows that the g-C_3N_4/TiO_2 heterostructure photoanode exhibits the lowest charge transfer resistance among all prepared photoanodes. This improved photoelectrochemical performance is attributed to the Z-scheme heterostructure generated by establishing an interfacial oxygen vacancy layer between TiO_2 and g-C_3N_4, and this interfacial layer promote the separation and transport of charge carriers. Subsequently, the author further confirmed the formation of this Z-scheme heterostructure through hydroxyl fluorescence capture and characterization and spin polarization DFT calculations.

6 Adsorption of water molecules on the surface of TiO_2 and the formation of hydrogen bonds

6.1 Adsorption of a single water molecule on the surface of TiO_2

In the photocatalytic water-splitting reaction, the adsorption state of water molecules on the surface of TiO_2 will directly affect its catalytic activity. Scholars in the field of theoretical calculations have conducted numerous studies on the interfacial adsorption configuration of water molecules and TiO_2, but controversies still exist regarding the adsorption morphology and structure of water molecules. The most controversial question is whether water molecules self-dissociate on the surface of TiO_2 [122,123]. This problem is important because the dissociated water molecules will provide TiO_2 an OH group adsorbed on the titanium atom on its surface, and the OH group on the surface of TiO_2 plays an important role in the photocatalytic reaction.

In recent years, the results of these theoretical calculations of the adsorption energy of the single water molecule in the molecular state and dissociated state on the surface of TiO_2 depend strongly on the selection of parameters, such as functionals, the number of layers of the TiO_2 surface model and crystal planes. For example, most of the results obtained from the RPBE functional calculations revealed a lower dissociative adsorption energy of water molecules, while the results of the PW91 and PBE functional calculations produced a lower molecular adsorption energy of water molecules. The number of layers of the TiO_2 surface model will also exert a substantial effect on the results of the theoretical calculations. As shown in Figure 4(a), Kowalski et al. [124] observed a strong odd–even oscillation behavior of the adsorption energy as the number of layers of the TiO_2 surface model changed. A similar oscillation behavior exists even on a clean TiO_2 surface, and the difference in the surface hybridization of Ti–O bonds between odd and even layers is the main explanation for this result [125]. In addition, as shown in Figure 4(b), Zhao [126] used DFT and reported that a single water molecule adsorbed on rutile phase TiO_2(100) is mainly in the molecular state, while dissociation state adsorption mainly occurred on the surface of (001) and (110), which was also confirmed by a series of subsequent studies [127,128]. Although the dissociation adsorption on the (110) surface is more stable, the reaction energy of the molecular adsorption structure and the dissociation adsorption structure are very similar, with a difference of only 0.089 eV.

In addition to calculating the surface adsorption energy of TiO_2, thermodynamic and kinetic studies also improve our understanding of the state of the single water molecule on the surface of TiO_2. Luo et al. [129] used a 3×2 primitive cell with 1/6 of the water molecular layer coverage and GGA functional calculation to obtain a water molecular splitting potential barrier of 0.20 eV, while the water molecular splitting potential barrier obtained using the GGA + U method and the same model is only 0.08 eV (Figure 4(c)). These low splitting potential barriers allow water molecules to dissociate on the TiO_2 surface with low coverage.

6.2 Adsorption of a single layer of water molecules on the surface of TiO_2

Similarly, in the field of theoretical calculations, researchers have also disputed whether the adsorption of the single layer of water molecules occurs in a molecular state or a dissociated state. Notably, when considering whether the single layer of water is dissociated on the surface of TiO_2 in a 1×1 surface primitive cell model, the molecular state

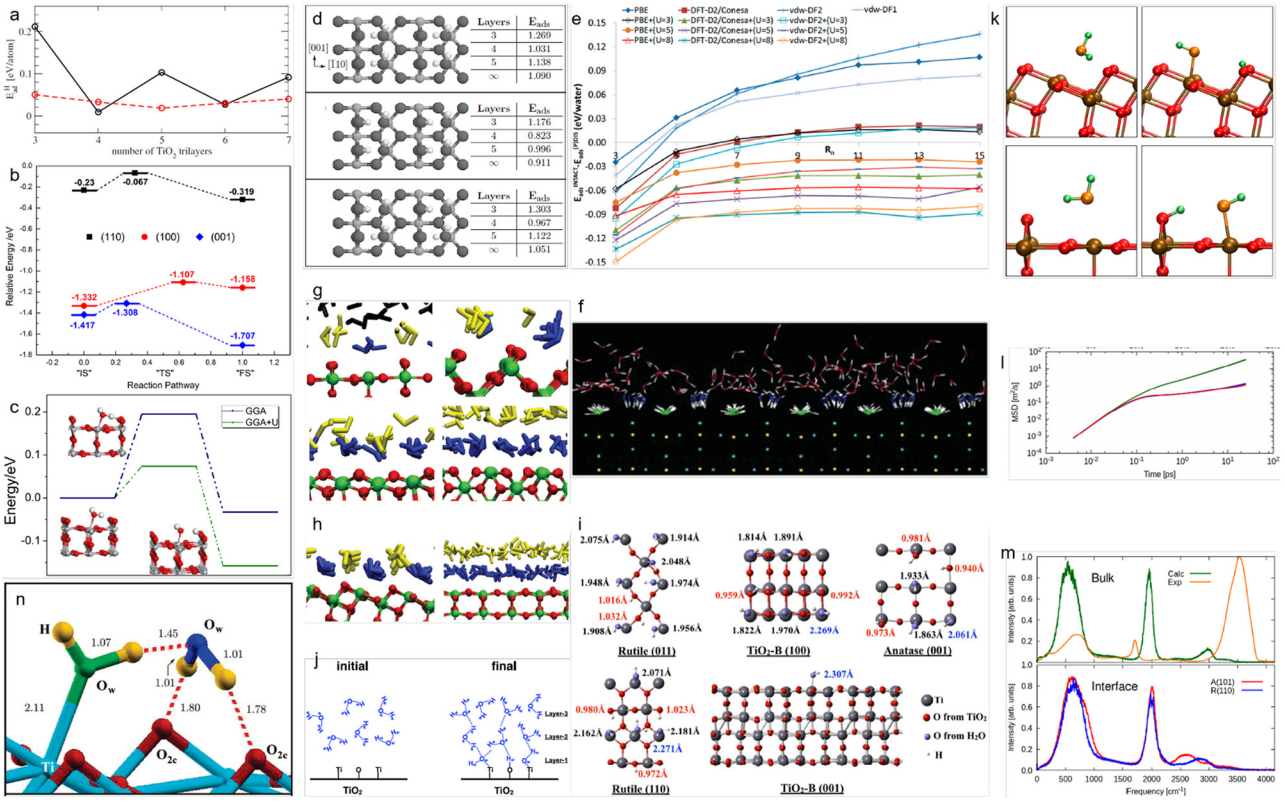

Figure 4: (a) Convergence of the hydrogen adsorption energy E_{ad}^{H} with slab thickness at full monolayer coverage, reprinted with permission from ref. [124], Copyright (2009) American Physical Society. (b) The comparison of decomposition reaction pathways of water on the low-index rutile TiO_2 surfaces, reprinted with permission from ref. [126], Copyright (2014) American Chemical Society. (c) Adsorption and dissociation of H_2O molecule at ground state calculated with GGA and GGA + *U* methods, reprinted with permission from ref. [129], Copyright (2013) American Chemical Society. (d) Plan view of the three 1 ML adsorption modes: molecular, dissociative, and "mixed", reprinted with permission from ref. [130], Copyright (2004) American Physical Society. (e) Difference in the adsorption energy between associated and partially dissociated configurations using various dispersion and DFT + *U* corrections with varying slab thicknesses, reprinted with permission from ref. [131], Copyright (2013) American Chemical Society. (f) MD snapshots of rutile hydrated surfaces, reprinted with permission from ref. [143], Copyright (2007) American Chemical Society. (g) Representative configurations of various rutile-water interfaces: (110), (100), (101), and (001), (h) Representative configurations of various anatase–water interfaces: (101) and (001), reprinted with permission from ref. [136], Copyright (2011) Taylor & Francis. (i) Partial final configurations of the five studied TiO_2/H_2O systems. (j) Cartoon illustration of the hydrogen bond network on reactive TiO_2 surfaces, reprinted with permission from ref. [146], Copyright (2014) American Chemical Society. (k) Dissociative adsorption of water on (a) anatase (101) and (b) rutile (110) surfaces, (l) on the logarithmic scale, where the transition from ballistic to the random-walk regime is clearly visible, and (m) IR spectrum of water calculated as a power spectrum of the system-collective-dipole autocorrelation function, reprinted with permission from ref. [147], Copyright (2017) American Chemical Society. (n) The structure and the difference density map of a pair of water molecules adsorbed on the (101) anatase surface are presented in parts, reprinted with permission from ref. [152], Copyright (2008) American Chemical Society.

of water molecules is unable to be described well. The choice of a surface primitive cell model exceeding 2 × 1 can avoid this problem well.

Analogously, the results of these theoretical calculations of the adsorption energies of the single layer of water molecules in the molecular state and dissociation state on the TiO_2 surface also depend on the selection of parameters, such as functionals and the number of layers of the TiO_2 surface model. As shown in Figure 4(d), Harris and Quong [130] used the PW91 functional and the surface primitive surface cell model (2 × 2) of TiO_2 with three layers for the calculation and found that the simultaneous presence of mixed adsorption state of the molecular state and the dissociated state is the most stable configuration. However, as the number of TiO_2 surface model layers continues to increase, the most stable state of the monolayer water molecules on the TiO_2 surface changes from a mixed adsorption state to a molecular adsorption state. As shown in Figure 4(e), Kumar et al. [131,132] used the functional with van der Waals correction to obtain the result that the single layer of water molecules does not dissociate when the number of TiO_2 surface model layers

is sufficient. In addition, the authors also considered the effect of the *U* value on the calculated result. When the *U* value is sufficiently large, the monolayer of water molecules will exist in the form of the mixed adsorption state. Notably, the selection of the appropriate empirical *U* value to accurately describe the properties of the TiO_2 surface is itself a very complicated problem. Some research groups have also used HFs [133,134] to study the monolayer of water molecules on the surface of TiO_2 and to solve the problem of an inaccurate description of the electronic molecules of semiconductors by GGA; all of these researchers have obtained a single conclusion that the monolayer of water molecules does not dissociate from the surface of TiO_2.

6.3 Multilayer structure of water molecules on the surface of TiO_2

In the actual photocatalytic water-splitting system, the surface of TiO_2 usually contacts water molecules with higher coverage. At this time, the water molecules easily form a highly ordered hierarchical structure on the surface of TiO_2, and this structure will follow the increase in the surface distance and gradually weaken. Since the time scale of the classical molecular dynamics simulation that can be calculated is longer [135] and the number of TiO_2 surface model layers is also increased, this review mainly introduces some reports on classical molecular dynamics simulation that strongly depend on the force field. The force fields currently used to simulate the system of TiO_2 and water molecules mainly include the Matsui Akaogi force field suitable for TiO_2, which is applicable to both the surface and bulk phase of TiO_2 [136]. In the water molecule model, TIP3P and SPC/E are the most widely used force fields [137–139]. The Buckingham potential and Lennard-Jones potential are usually used to describe the interaction between water molecules and the TiO_2 surface [140–142].

As shown in Figure 4(f), Mamontov et al. [143] performed classical molecular dynamics simulations and found that water molecules were stratified on the surface of rutile phase TiO_2(110), forming a three-layer structure. Among these layers, the oxygen atoms in the first layer of water molecules exert a strong effect on the Ti atoms on the surface of TiO_2; the hydrogen atoms in the second layer of water molecules exert a strong effect on the oxygen atoms on the surface of TiO_2. Both the first and second layers of water molecules have formed a highly ordered structure and are stably adsorbed on the (110) crystal face of TiO_2, while the third layer of water molecules is rarely affected by the surface, consistent with the results of the molecular dynamics simulation reported by Kavathekar et al. [136]. Furthermore, the authors also studied the distributed structure of water molecules on other crystal faces of rutile phase TiO_2 and anatase phase TiO_2. Water molecules will also form a double-layer ordered structure on the other crystal faces (Figure 4(g) and (h)).

On the other hand, the development of the reaction force field provides a new theoretical approach for studying the interfacial characteristics of TiO_2 and water molecules [144,145]. As shown in Figure 4(i), Huang et al. [146] used the reaction force field (ReaxFF) to analyze the structure of water molecules on the surface of TiO_2 and their dissociation and adsorption. The dissociation adsorption of water molecules occurred near the rutile phase TiO_2(110), (011), anatase phase TiO_2(001) and TiO_2-B(100) crystal faces, while only molecular adsorption was observed at the crystal surface of TiO_2-B(001). As shown in Figure 4(j), water molecules form a three-layered, ordered structure on the rutile TiO_2(011) crystal face. Futera et al. [147] studied the static and dynamic structural characteristics of the anatase TiO_2(101) crystal face, rutile TiO_2(110) crystal face, and the water molecule interface using ReaxFF. The results of the theoretical calculation revealed a clear, layered, and well-organized structure of water molecules in the interface area within the range of 6.5 Å from the TiO_2 surface. The molecules of the first hydration layer adsorbed on the unsaturated surface titanium atoms will spontaneously dissociate, but controversy exists regarding whether H^+ will completely cover O_{2c}/O_b and OH^- will partially cover Ti_{5c} (Figure 4(k)). Moreover, the expected change in the inherent electric field in the interface was large, and the drop in the electrostatic potential was also large. The interfacial water is severely restricted, and its self-diffusion constant is two orders of magnitude lower than the 2.28×10^{-9} m^2/s constant reported for the bulk water (Figure 4(l)). The pivoted motion of adsorbed water molecules is also considerably hindered. The author also calculated that the hydrogen bond lifetime on the interface is also shorter than in the bulk water region. Finally, the Fourier transform infrared (FT-IR) spectra procured from the collective water dipole changes in the interface area revealed a stronger effect of water molecules on the stretching vibration of the anatase (101) crystal plane than on the rutile (110) crystal plane (Figure 4(m)). However, the detection of the presence of the liquid water bond stretching

vibration is often limited by the loss of accuracy of the applied reaction potential.

6.4 Hydrogen bonds formed by water molecules on the surface of TiO_2

At the interface between TiO_2 and water molecules, the possible hydrogen bonding sites are mainly observed between two water molecules and the H atom in the water molecule and between dissociated H^+, dissociated OH^- and O atoms on the surface of TiO_2. The strength of the hydrogen bond formed will also exert a certain effect on the structure of water molecules formed on the surface of TiO_2 [148,149]. Kumar et al. [150] used first-principles molecular dynamics simulations to calculate the various hydrogen bonds formed during the interaction of water molecules with the surface of TiO_2. Table 1 presents the structural information of the four types of hydrogen bonds with the strongest acting force.

Similarly, English [151] performed FT-IR spectroscopy and found that in the wavelength range of 835 to 920 cm^{-1}, water molecules formed stable hydrogen bonds with the surface of rutile phase TiO_2, while the oxygen vacancy on the surface of TiO_2 formed weak hydrogen bonds with water molecules and bridged oxygen atoms on the surface. As shown in Figure 4(n), the results of the calculations performed by Mattioli et al. [152] using DFT and first-principles molecular dynamics simulations reveal that the hydrogen bond formed by water molecules on the surface of the anatase phase TiO_2(101) is stronger than the bond formed on the surface of the rutile phase, and the role of hydrogen bonding in the permutation of atoms on the surface of TiO_2 and the vibration characteristics of intermediate products in the water-splitting process is very important. Additionally, the selection of crystal planes will also exert a certain effect on the stability of hydrogen bonds. This point was also confirmed in a subsequent study by English et al. [153]. The authors simulated the molecular dynamics of hydrogen bonds formed by water molecules and rutile TiO_2(110), (101), (100) and anatase TiO_2(101) crystal faces at room temperature. The hydrogen bonds on the anatase phase TiO_2(101) crystal planes were the most stable, followed by the rutile phase TiO_2(110) crystal planes. Water molecules adsorbed on these crystal faces potentially increase the number of hydrogen bonds and their stability, particularly on the surface of anatase phase TiO_2, which may be beneficial to accelerate the activity of TiO_2 for water splitting.

7 Rate-limiting step of the water-splitting reaction on the surface of TiO_2

The photocatalytic water-splitting reaction on the surface of TiO_2 is composed of several different elementary reactions [154–156]. In previous studies, the energy barrier to be overcome during the reaction was one of the main factors affecting the reaction [157]. As the OER is the most important process [158], many researchers have conducted many theoretical reports on the OER mechanism in the last 10 years [159,160]. As shown in Figure 5(a), Hu et al. [158] used a first-principles method to study the photocatalytic OER at the water/TiO_2(110) interface. Theoretical calculations show that all factors affecting the OER rate will vary with the concentration of photogenerated holes (C_{h^+}) reaching the surface of TiO_2. Under the experimental conditions, the intrinsic catalytic activity of TiO_2(110) is not the major factor that alters the increase in the OER rate, as all steps involving photogenerated holes are very slow due to the low C_{h^+} reaching the surface of TiO_2 (Figure 5(b)–(d)). Therefore, the key to improving the efficiency of OER is to increase C_{h^+} reaching the surface of TiO_2 as much as possible toward its estimation threshold ($C_{h^+} \approx 10^{-4}$). Lang et al. [161] thoroughly studied the mechanism of OER on the TiO_2(001) crystal plane covered by water. The authors discovered a novel OER pathway on the (001) crystal plane, namely, the straight transfer of protons from molecular water and surface hydroxyl groups, as well as the O–O coupling process. In this pathway, the O–O coupling step exhibits the largest

Table 1: Characteristics of the strongest hydrogen bonds in the H_2O/TiO_2 interface

H-bond	configuration	*d* relaxed (Å)	*d* range (Å)	*d* peak (Å)	*d* range (Å)	frequency (THz)
Ti_2**O**H-H**O**H	M_2(1)	1.74	1.6–2.1	1.66	1.4–1.9	92.5
Ti_2**O**-H**O**H	M_2(2)	1.77	1.4–1.9	1.63	1.4–2.0	93.9
TiHO**H**-H**O**H	M_2(2)	1.76	1.4–1.8	1.66	1.4–2.0	92.4
Ti**O**H-**H**OH	M_2(1)			1.70	1.4–2.0	92.4

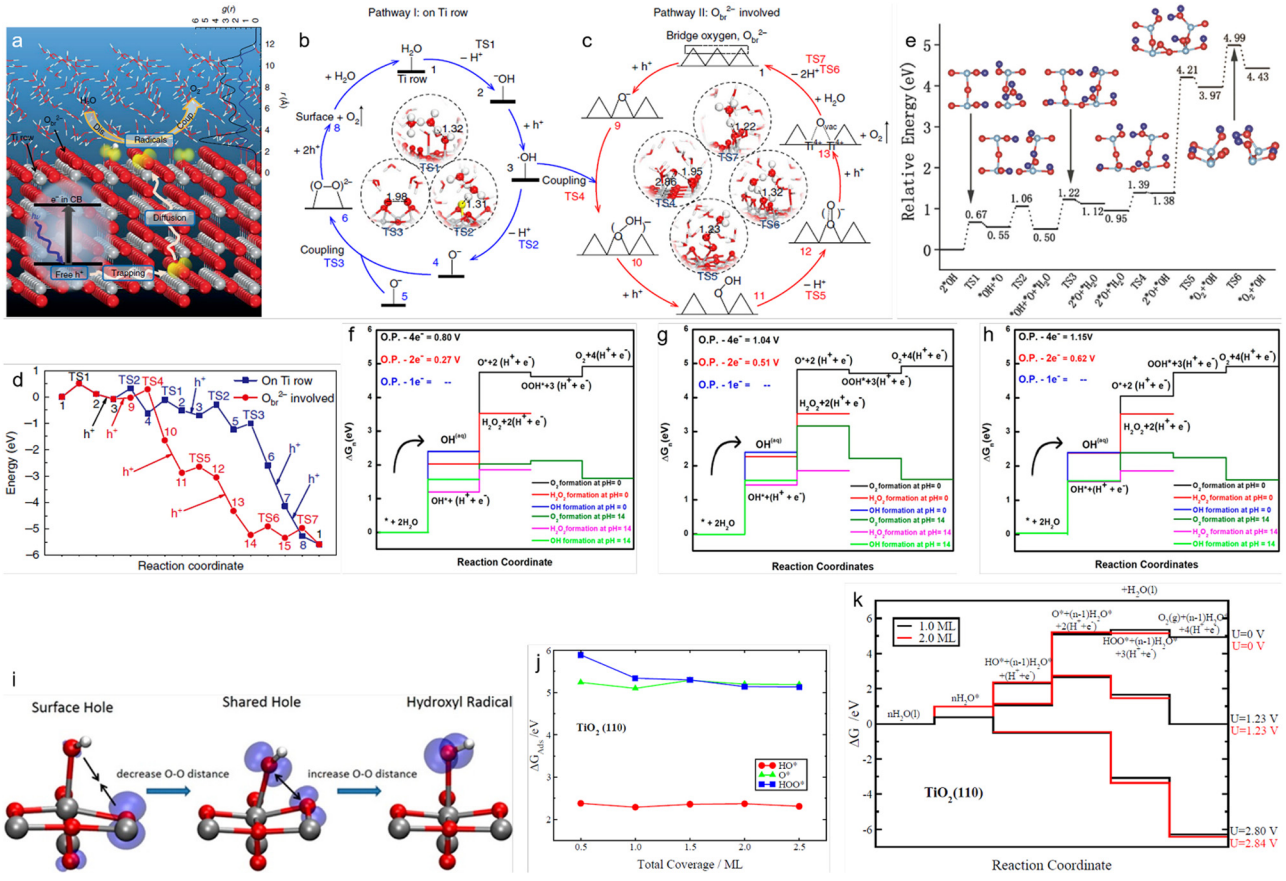

Figure 5: (a) Schematic of the photocatalytic OER at the water/TiO_2 interface and proposed mechanism of the dual pathways for photocatalytic OER: (b) pathway I: occurring on the Ti row and (c) pathway II: involving bridge oxygen. (d) The energy profiles of pathways I and II, reprinted with permission from ref. [158], Copyright (2018) Springer Nature. (e) Calculated potential energy profiles of these elementary steps during H_2O oxidation to O_2 on the unreconstructed TiO_2(001) surface, reprinted with permission from ref. [161], Copyright (2020) Royal Society of Chemistry. Free energy diagrams for the OER through peroxo O2* species on (f) TiO_2 rutile (110), (g) anatase (101), and (h) brookite (210) phases, reprinted with permission from ref. [16], Copyright (2020) American Chemical Society. (i) The rate-limiting steps in the water-splitting reaction process on the TiO_2 surface, reprinted with permission from ref. [164] Copyright (2013) American Chemical Society. (j) Calculated free energy for OER intermediates as a function of total coverage and (k) calculated free energy diagram for OER on the defect-free TiO_2(110) surface covered with water, reprinted with permission from ref. [165], Copyright (2014) American Chemical Society.

thermodynamic energy and the highest energy barrier, indicating that this process is the rate-limiting step in the entire approach (Figure 5(e)). The authors' discovery provides novel insights into the strong dependence of the water adsorption mode of the anatase phase TiO_2(001) crystal plane on the coverage rate, and they attempted to explain the strong oxidation activity on the surface of TiO_2(001) in a representative photocatalytic water-splitting environment. Liu et al. [16] systematically and comparatively studied the mechanism and energetics of water oxidation on the surface of rutile phase TiO_2(110), anatase phase TiO_2(101), and brookite phase TiO_2(210) models using DFT. The results of the theoretical calculation show that the easiest mechanism for water oxidation on these three different crystalline phases is the formation of H_2O_2 double electrons/protons through surface peroxide O* intermediates. As shown in Figure 5(f)–(h), the calculated overall overpotentials for H_2O_2 formation on the rutile phase, anatase phase, and brookite phase are approximately 0.27, 0.51, and 0.62 V, respectively, and the rate-limiting step for H_2O_2 formation is the OH* constitution step for the three types of crystalline phases. The author also examined the effects of pH. The pH value changes the binding energy of the reaction intermediate and alters the thresholds of the 1-e, 2-e, and 4-e processes, but does not influence the selectivity. The overpotentials of the 4-e O-2 evolution are 0.8, 1.04, and 1.15 V on the rutile phase, anatase phase, and brookite phase, respectively, with the uniform rate-limiting step identified as the 2-e process.

Additionally, Li et al. [162] researched the crystal faces of anatase phase (101) and (001) and found that the decomposition reaction of water on the surface is

not subtle to the local surface structure. In addition, the authors also concluded that the overpotential of the reaction is mainly affected by the position of the top of the VB. In the reaction process, the main rate-limiting step is the formation of hydroxyl radicals (OH*) from the water molecules and the vacancy of the TiO_2 surface. This point was also confirmed in the study by Valdes et al. [163]. As shown in Figure 5(i), Chen et al. [164] performed a detailed kinetic analysis of the rate-limiting steps in the water-splitting reaction on the TiO_2 surface based on the theoretical calculations using DFT. The reaction is accompanied by the continuous electron transfer process of proton coupling, and proton transfer precedes electron transfer. As shown in Figure 5(j), Siahrostami and Vojvodic [165] analyzed the effect of water coverage on the rutile TiO_2(110) crystal surface on the reaction energy barrier. In the four elementary reactions, the coverage of water had little effect on the formation of (O*) and (HO*), but it significantly reduced the reaction energy barrier for the formation of (HOO*) (Figure 5(k)).

In summary, the reaction kinetics of water splitting on the TiO_2 surface are mainly determined by the rate-limiting steps of the elementary reaction in the process, and the difficulty of the elementary reaction is determined by the free energy of the reaction. The water coverage on the surface of TiO_2 will also exert a certain effect on the size of the reaction energy barrier.

8 Charge transfer process occurring on the surface of TiO_2

In the photocatalytic reaction process, the effective utilization of the photogenerated electron–hole pair of TiO_2 is an important factor affecting its photochemical performance, and it is the pivotal to improving the efficiency of TiO_2 photocatalytic water-splitting reaction to produce hydrogen. When TiO_2 is excited by incident light, the photogenerated electrons will transition and be injected into the CB of TiO_2. Then, these electrons either migrate to the surface of TiO_2 through diffusion and are effectively used, are captured by the defect state of the TiO_2 surface, or recombine with the positive charge of the electrolyte or the sensitizer. The aforementioned processes all occur simultaneously.

According to experimental [166,167] and theoretical studies [168,169], photogenerated electrons are trapped by defects on the TiO_2 surface. As shown in Figure 6(a), Luo et al. [170] used DFT to show that photogenerated holes on the rutile TiO_2(110) crystal plane are more likely to be adsorbed by the bridge oxygen atoms and have the characteristics of p orbitals. When interacting with water molecules on the surface of TiO_2, the holes will hybridize with the highest occupied orbital of water molecules (Figure 6(b)). Furthermore, based on the simultaneous removal of a proton and electron from the crystal face of rutile TiO_2(110) and the maintenance of the neutrality of the unit cell, Cheng et al. [171] established a surface model of photogenerated holes and analyzed the different positions where holes are trapped on the surface and their energy maps by performing DFT calculations. Among these positions, $TiOH^{\cdot}$ and TiO^{-} are the most stable hole trap sites (Figure 6(c)).

Minot et al. [172] established a model of the photoexcited state at the interface between water molecules and TiO_2. DFT calculations found that the photogenerated electrons are located on the five-coordinated Ti atom on the TiO_2 surface, while the holes are located between two oxygen atoms adjacent to the Ti atom. Moreover, the concentration of electron–hole pairs on the surface of TiO_2 is related to the size of the unit cell, as a smaller size results in a higher concentration. As shown in Figure 6(d), Nakamura et al. [173] conducted a DFT calculation to study the photoexcited solvated electrons on the interface of water molecules and TiO_2 and found that the distribution of solvated electrons on the interface is mainly affected by the hydrogen bonds on the interface. This electron is mainly distributed around the dangling hydrogen bond, and a type of "wet electron" is formed. Prezhdo et al. [174] also used the DFT method to study "wet electrons." Figure 6(e) shows the process by which "wet electrons" are generated by photogenerated electrons at the interface of water molecules and TiO_2 to the surface state to the bulk phase. Due to the strong coupling between the surface of TiO_2 and water molecules, the electron transfer process is extremely fast, but the adiabatic mechanism and the nonadiabatic mechanism contribute equally to electron transfer. Compared with the vibration of the hydroxyl group, the motion of water molecules exerts a greater effect on the electron transfer dynamics. This "wet electron" represents the lowest energy path for electron transfer at the interface of the metal oxide and aqueous solution. It may play important role in photocatalysis and the photoelectrochemical energy conversion process of TiO_2 and other oxides [175].

Zhao et al. [176] studied the interaction between graphene and anatase phase TiO_2(110) crystal planes with or without oxygen vacancies using first-principles calculations. The tight but nondestructive contact at the interface promotes the transfer of photoexcited electrons between graphene and TiO_2. Since the work function is smaller than a TiO_2 substrate without oxygen vacancies, graphene

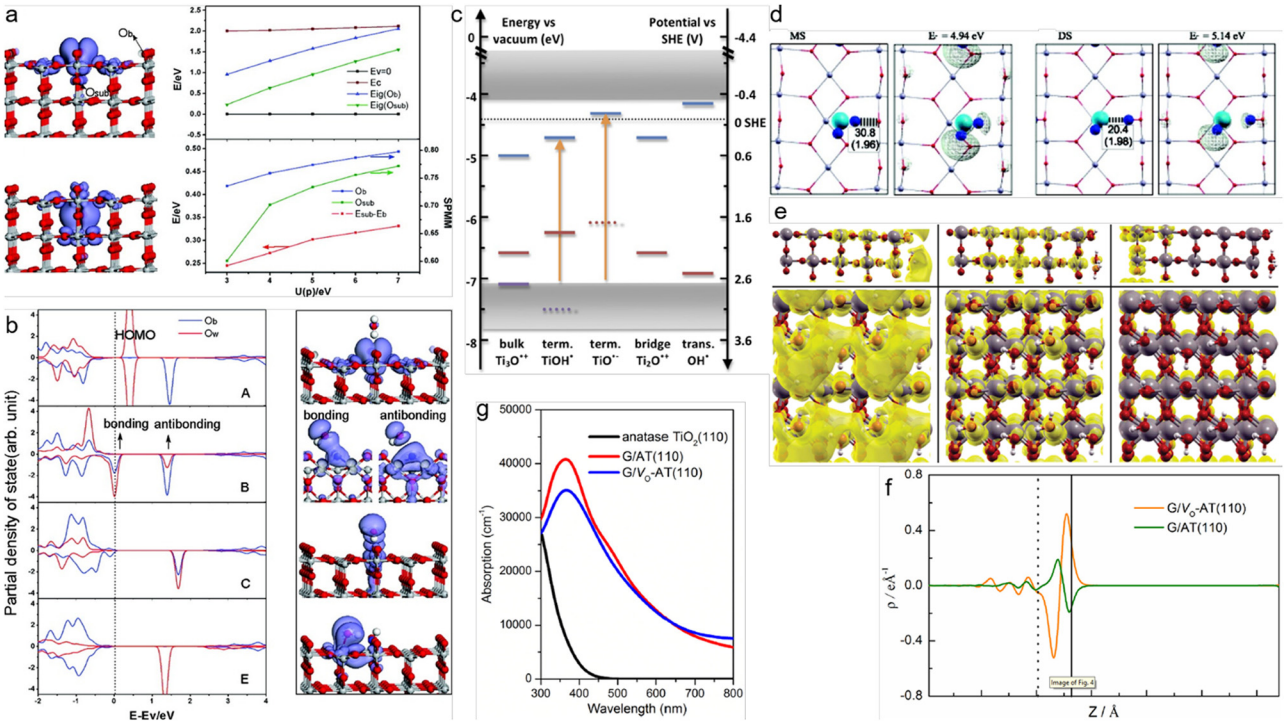

Figure 6: (a) Iso-density surface of hole orbital trapped at O_b and O_{sub}, the dependence of eigenvalues of the hole orbital trapped at O_b and O_{sub}, SPMM of O_b and O_{sub} and relative energy for hole trapping at these two sides, (b) PDOS of O_b and O_w in the states A, B, C, and E, and corresponding iso-density surface of trapped hole orbital, reprinted with permission from ref. [170], Copyright (2012) American Chemical Society. (c) Alignment of the vertical and adiabatic electronic energy levels for the trapped holes in TiO_2, reprinted with permission from ref. [171], Copyright (2014) American Chemical Society. (d) The optimized H_2O adsorption structures for the molecular adsorption and dissociative adsorption models, reprinted with permission from ref. [173], Copyright (2009) American Chemical Society. (e) Charge densities for the wet electron state (left panel), the surface state (middle panel), and the bulk state (right panel) of the wet electron system, reprinted with permission from ref. [174], Copyright (2009) American Chemical Society. (f) The planar averaged charge density difference along the direction perpendicular to the graphene slab. (g) Calculated part of the UV–vis absorption spectra, reprinted with permission from ref. [176], Copyright (2017) Elsevier.

usually depletes electrons. However, the introduction of surface oxygen vacancies significantly reduces the work function of TiO_2 to a smaller value than graphene, which causes electrons to reverse their transfer and accumulate on the graphene sheet (Figure 6(f)). In particular, as shown in Figure 6(g), the obvious redshift of the optical absorption edge and the markedly reinforced absorption intensity in the visible light region of graphene/anatase phase TiO_2 with or without oxygen vacancies illustrates the escalation mechanism of the photocatalytic efficiency of TiO_2.

In summary, DFT is mainly used for the simulation and calculation of the charge transfer process on the TiO_2 surface. By establishing the photoinduced excited state model and the photogenerated hole model on the interface of water molecules and TiO_2, relevant information, such as the electron trapping sites, the hole trapping sites, and the concentration of electron–hole pairs, can be obtained, and the lowest energy path theory using "wet electrons" for electron transfer at the interface of water molecules and TiO_2 may help researchers analyze the process of photocatalysis water-splitting energy conversion. In addition, the loading of some cocatalysts on the surface of TiO_2, such as graphene, also helps promote the transfer of photogenerated charges on its surface.

9 Application of theoretical calculations to TiO_2-based commercial photocatalysts for hydrogen production through a water-splitting reaction

As the most promising photocatalyst for hydrogen production mediated by water splitting, TiO_2 has already

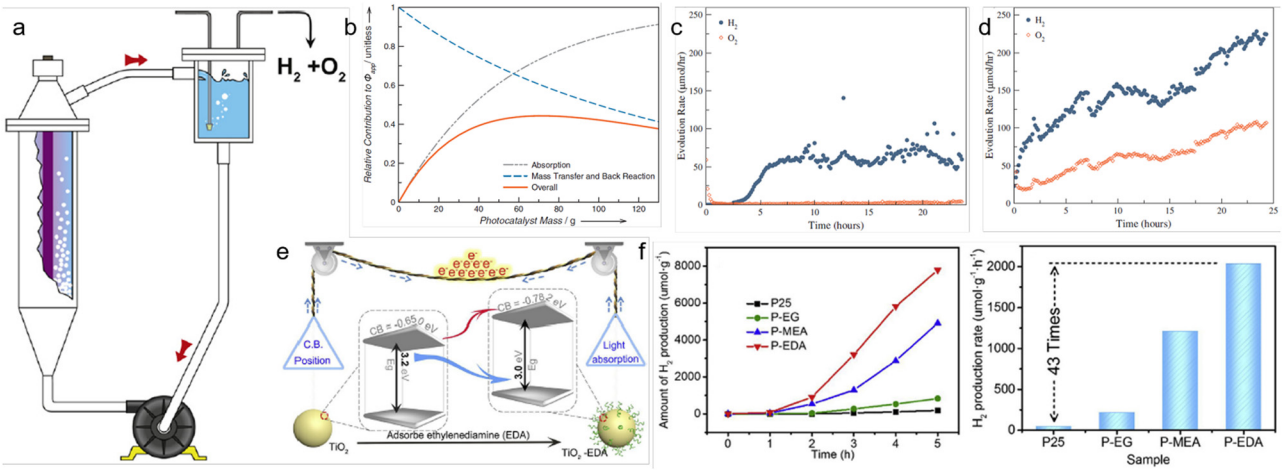

Figure 7: (a) Schematic of the photocatalytic water-splitting reaction in a fluidized bed system. (b) The individual contributions of photon absorption, mass transfer, and the back reaction to the apparent quantum efficiency as a function of photocatalyst mass. The rate of hydrogen and oxygen evolution over time (c) under normal conditions and (d) after improving turbulence and liquid–gas contact, reprinted with permission from ref. [177], Copyright (2018) Elsevier. (e) Schematic of the general procedure used to prepare the target photocatalysts P-EDA. (f) The photocatalytic hydrogen production curve and the rate histogram of samples, reprinted with permission from ref. [178], Copyright (2020) Elsevier.

emerged in commercial applications. Many theoretical calculations for its commercial application have appeared in recent years to facilitate the commercialization of TiO_2-based photocatalysts.

As shown in Figure 7(a), Taghipour et al. [177] combined the fluidized bed theory, mass transfer effect, optical model, and catalytic reverse reaction of hydrogen and oxygen dominated by the noble metal Pt loaded on the surface of TiO_2 and established a model for describing the property of photocatalytic water splitting in fluidized bed systems (Figure 7(b)). The model estimates a series of model parameters and accurately predicts the hydrogen release rate of a given mass of Pt/TiO_2 granules and an extended bed height. Subsequently, based on the model, the hydrogen evolution rate and apparent quantum efficiency of the system are rapidly dominated by the mass transfer rate in the separator. If the gas–liquid separator is optimized or the fluidization flow is increased to ensure that the mass transfer rate is far greater than the reverse reaction rate of H_2 and O_2 catalyzed by Pt, the performance of the system will be maximized (Figure 7(c) and (d)). The author also confirmed this inference through experimental verification of the model, as a small improvement in the separation device increased the hydrogen evolution rate of the system by 350%. As a formidable tool for designing and optimizing photocatalytic fluidized bed systems, this model not only maintains the property of existing TiO_2-based photocatalysts but also minimize the energy required to produce hydrogen.

As shown in Figure 7(e), Hu et al. [178] used a simple mechanical lapping method to attach organics with electron supply capabilities to the surface of commercial P25. The results of the theoretical calculation show that the electron-donating organic matter attached to the surface of commercial P25 produces more electrons. These electrons expand the range of light absorbed by commercial P25 via impeding the attraction of holes to photoinduced electrons and improving the separation efficiency of its photogenerated current carriers. The property of the commercial P25 photocatalytic water-splitting reaction for hydrogen production has also been significantly improved, with a continuous increase in the electron-donating capacity of functional groups in organics, from small to large: PeEG < P-MEA < P-EDA. Among these functional groups, P-EDA has the highest yield of H_2 that is 43 times higher than the marketed P25 (Figure 7(f)). This study may result in the development of a new field for the commercialization of TiO_2 designed to enhance the performance of photocatalytic water-splitting reactions to produce hydrogen by attaching various organic substances to the surface of TiO_2-based photocatalysts.

10 Conclusions and future development directions

10.1 Conclusions

As the most promising semiconductor material for photocatalytic water-splitting reactions, TiO_2-based nanomaterials have received extensive attention from researchers

in academia and industry in recent years. This review describes the research progress in theoretical calculations related to TiO_2-based photocatalytic water splitting, focusing on the analysis of the adsorption state of water molecules with different levels of coverage on the TiO_2 surface, the rate-limiting steps of the decomposition of water molecules on the TiO_2 surface, and the transfer process of photoexcited carriers at the interface between water molecules and TiO_2. Finally, a brief introduction of the theoretical calculations of TiO_2-based commercial photocatalysts in water splitting is provided.

10.2 Existing problems

The theoretical calculation of TiO_2-based photocatalytic water splitting is currently limited to only pure TiO_2 or a relatively simple system, such as elemental doping or metal loading of TiO_2. Some studies involving more complex photocatalytic systems, such as heterojunction systems of TiO_2 and other semiconductors, have mostly focused on the experimental aspect, and relatively few applications in photocatalytic water-splitting reactions for hydrogen production have been reported; thus, studies of theoretical calculations are even less frequently reported.

10.3 Future development directions

The microstructure and related properties of the heterojunction interface formed by TiO_2 and other semiconductors require further study to solve these problems. For a photocatalytic system, the system is in a nonequilibrium state throughout the process from the absorption of photons to the excitation of electrons and holes to the various behaviors of electrons and holes after excitation. A very accurate description of the electronic structure and electronic vibration dynamics is needed for theoretical calculations to simulate the nonequilibrium state process occurring at the molecular scale and nanoscale at the atomic level. In other words, the appropriate crosslinking function and density functionals must be studied to more accurately describe long-range electron transport, multielectron excited states, bond breakage, and other situations that create the nonequilibrium state of the system.

The development of time-domain (TD) DFT and nonadiabatic molecular dynamics theory [179–182] describes the time scale for the photoexcited electron transport, energy transport, thermal relaxation and charge recombination processes that occur on the photocatalytic interface system. Simulation calculations provide the conditions [183–185]. At the same time, this method also provides unique and universal theoretical support for studies of different nonequilibrium processes that occur in photocatalytic systems. However, the theory is only able to provide theoretical calculations for smaller systems at present, and the simulation time scale is only a few hundred picoseconds. Therefore, the further development of this theory for application to more complex photocatalytic systems will be the focus of future research. On the other hand, the in-depth understanding of the interface properties and the charge behavior at the interface of the heterojunction formed by TiO_2 and other semiconductors through simulations and calculations will provide a solid theoretical basis for the design of the architecture, and TiO_2-based photocatalytic water splitting represents a new method to improve the efficiency of hydrogen production.

Acknowledgments: This work was funded by National Natural Science Foundation of China, grant number 51875008, and basic financial support from Beijing Municipal Education Commission.

Conflict of interest: The authors declare no conflict of interest regarding the publication of this paper.

References

[1] Fujishima A, Honda K. Electrochemical photolysis of water at a semiconductor electrode. Nature. 1972;238(5358):37–8.

[2] Yousefian R, Emadoddin E, Baharnezhad S. Manufacturing of the aluminum metal-matrix composite reinforced with micro- and nanoparticles of TiO_2 through accumulative roll bonding process (Arb). Rev Adv Mater Sci. 2018;55(1):1–11.

[3] Boufi S, Bouattour S, Ferraria AM, Ferreira LFV, do Rego AMB, Chehimi MM, et al. Cotton fibres functionalized with plasmonic nanoparticles to promote the destruction of harmful molecules: An overview. Nanotechnol Rev. 2019;8(1):671–80.

[4] Park H, Kim HI, Moon G, Choi W. Photoinduced charge transfer processes in solar photocatalysis based on modified TiO_2. Energ Env Sci. 2016;9(2):411–33.

[5] Typek J, Guskos N, Zolnierkiewicz G, Pilarska M, Guskos A, Kusiak-Nejman E, et al. Magnetic properties of TiO_2/graphitic carbon nanocomposites. Rev Adv Mater Sci. 2019;58(1):107–22.

[6] Khitab A, Ahmad S, Munir MJ, Kazmi SMS, Arshad T, Khushnood RA. Synthesis and applications of nano titania particles: A review. Rev Adv Mater Sci. 2018;53(1):90–105.

[7] Qi K, Selvaraj R, Fahdi TA, Al-Kindy S, Kim Y, Wang G, et al. Enhanced photocatalytic activity of anatase-TiO_2

nanoparticles by fullerene modification: A theoretical and experimental study. Appl Surf Sci. 2016;387:750–8.
[8] Mazierski P, Lisowski W, Grzyb T, Winiarski MJ, Klimczuk T, Mikolajczyk A, et al. Enhanced photocatalytic properties of lanthanide-TiO_2 nanotubes: An experimental and theoretical study. Appl Catal B-Environ. 2017;205:376–85.
[9] Assadi MH, Hanaor D. The effects of copper doping on photocatalytic activity at (101) planes of anatase TiO_2: A theoretical study. Appl Surf Sci. 2016;387:682–9.
[10] Luo Z, Wang Z, Li J, Yang K, Zhou G. N-Promoted Ru-1/TiO_2 single-atom catalysts for photocatalytic water splitting for hydrogen production: A density functional theory study. Phys Chem Chem Phys. 2020;22:11392–9.
[11] Yao G, Zhao Z, Liu Q, Dong X, Zhao Q. Theoretical calculations for localized surface plasmon resonance effects of Cu/TiO_2 nanosphere: Generation, modulation, and application in photocatalysis. Sol Energ Mat Sol C. 2020;208:110385.
[12] Zhuang P, Yue H, Dong H, Zhou X. Effects of a Ni cocatalyst on the photocatalytic hydrogen evolution reaction of anatase TiO_2 by first-principles calculations. N J Chem. 2020;44: 5428–37.
[13] Harb M, Jeantelot G, Basset J. Insights into the most suitable TiO_2 surfaces for photocatalytic O_2 and H_2 evolution reactions from DFT calculations. J Phys Chem C. 2019;123(46): 28210–8.
[14] Nam Y, Lim JH, Ko KC, Lee JY. Photocatalytic activity of TiO_2 nanoparticles: A theoretical aspect. J Mater Chem A. 2019;7(23):13833–59.
[15] Zhu Y, Teobaldi G, Liu L. Water-hydrogen-polaron coupling at anatase TiO_2(101) surfaces: A hybrid density functional theory study. J Phys Chem Lett. 2020;11:4317–25.
[16] Malik AS, Liu T, Dupuis M, Li R, Li C. Water oxidation on TiO_2: A comparative DFT study of 1e(−), 2e(−), and 4e(−) processes on rutile, anatase, and brookite. J Phys Chem C. 2020;9:11450.
[17] Orhan OK, Oregan DD. First-principles Hubbard *U* and Hund's J corrected approximate density-functional theory predicts an accurate fundamental gap in rutile and anatase TiO_2. Phys Rev B. 2020;101:245137.
[18] Bahramian A. Molecular interactions insights underlying temperature-dependent structure of water molecules on TiO_2 nanostructured film: A computational study using reactive and non-reactive force fields. Fluid Phase Equilibr. 2017;438:53–66.
[19] Lei L, Sang L, Zhang Y, Gao Y. Interfacial analysis of anatase TiO_2 in KOH solution by molecular dynamics simulations and photoelectrochemical experiments. ACS Omega. 2020;5:3522–32.
[20] Sun K, Su H, Li W. Structures and stability of adsorbed methanol on TiO_2(110) surface studied by *ab initio* thermodynamics and kinetic Monte Carlo simulation. Theor Chem Acc. 2018;137(10):128.
[21] Luo Z, Wang Z, Li J, Yang K, Zhou G. N-Promoted Ru_1/TiO_2 single-atom catalysts for photocatalytic water splitting for hydrogen production: A density functional theory study. PhysChemChemPhys. 2020;22:11392.
[22] Liu J, Gong X, Alexandrova AN. Mechanism of CO_2 photocatalytic reduction to methane and methanol on defected anatase TiO_2(101): A density functional theory study. J Phys Chem C. 2019;123(6):3505–11.
[23] Morita K, Yasuoka K. Density functional theory study of atomic and electronic properties of defects in reduced anatase TiO_2 nanocrystals. AIP Adv. 2018;8(3):035119.
[24] Li H, Zhang X, Liu QJ, Liu YY, Liu HF, Wang XQ, et al. First-principles calculations of mechanical and thermodynamic properties of tungsten-based alloy. Nanotechnol Rev. 2019;8(1):258–65.
[25] Li W, Zhao Y, Wang T. Study of Pb ion adsorption on (n, 0) CNTs (n = 4, 5, 6). Nanotechnol Rev. 2018;7(6): 469–73.
[26] Lonsdale R, Fort RM, Rydberg P, Harvey JN, Mulholland AJ. Quantum mechanics/molecular mechanics modeling of drug metabolism: Mexiletine *N*-hydroxylation by cytochrome P450 1A2. Chem Res Toxicol. 2016;29(6):963–71.
[27] Michalowski M. Simulation model for frictional contact of two elastic surfaces in micro/nanoscale and its validation. Nanotechnol Rev. 2018;7(5):355–63.
[28] Bao G, Suresh S. Cell and molecular mechanics of biological materials. Nat Mater. 2003;2(11):715–25.
[29] Yan C, Zeng Q, Zhu J, Cao Q. Influence of Zr-S co-doping on the electronic structure and optical properties of anatase TiO_2: First-principles GGA plus *U* method. Appl Phys A-Mater. 2019;125(2):121.
[30] Han F, Zhou Z, Huang Z, Li M, Guo L. Effect of water adsorption on the interfacial structure and band edge alignment of anatase TiO_2(001)/water by first-principles molecular dynamics. J Phys Chem C. 2018;122(47):26965–73.
[31] Agosta L, Brandt EG, Lyubartsev AP. Diffusion and reaction pathways of water near fully hydrated TiO_2 surfaces from *ab initio* molecular dynamics. J Chem Phys. 2017;147(2):024704.
[32] Ariyanti D, Mukhtar S, Ahmed N, Liu Z, Dong J, Gao W. Surface modification of TiO_2 for visible light photocatalysis: Experimental and theoretical calculations of its electronic and optical properties. Int J Mod Phys B. 2020;34(1–3): 2040067.
[33] Ibrahim Q, Akbarzadeh R. A photocatalytic TiO_2/graphene bilayer membrane design for water desalination: A molecular dynamic simulation. J Mol Model. 2020;26:165.
[34] Alotaibi AM, Williamson BA, Sathasivam S, Kafizas A, Alqahtani M, Sotelo-Vazquez C, et al. Enhanced photocatalytic and antibacterial ability of Cu-doped anatase TiO_2 thin films: Theory and experiment. ACS Appl Mater Inter. 2020;12:15348–61.
[35] Harb M, Jeantelot G, Basset J. Insights into the most suitable TiO_2 surfaces for photocatalytic O_2 and H_2 evolution reactions from DFT calculations. J Phys Chem C. 2019;123(46): 28210–8.
[36] Xie X, Xiao P, Fang W, Cui G, Thiel W. Probing photocatalytic nitrogen reduction to ammonia with water on the rutile TiO_2(110) surface by first-principles calculations. ACS Catal. 2019;9(10):9178–87.
[37] Ganguly P, Mathew S, Clarizia L, Kumar RS, Akande A, Hinder S, et al. Theoretical and experimental investigation of visible light responsive $AgBiS_2$-TiO_2 heterojunctions for enhanced photocatalytic applications. Appl Catal B-Environ. 2019;253:401–18.
[38] Chang J, Jiang Z, Zhang Z, Lin Y, Tian P, Zhou B, et al. Theoretical studies of photocatalytic behaviors of isoelectronic C/Si/Ge/Sn-doped TiO_2: DFT + *U*. Appl Surf Sci. 2019;484(AUG.1):1304–9.

[39] Aschauer UJ, Tilocca A, Selloni A. *Ab initio* simulations of the structure of thin water layers on defective anatase TiO_2(101) surfaces. Int J Quant Chem. 2015;115(18):1250–7.
[40] Zhao Y, Wang W, He L. The effects of Co/N dopants on the electronic, redox potential, optical, and photocatalytic water-splitting properties of TiO_2: First principles calculations. Chem Phys Lett. 2017;685:108–13.
[41] Shi H, Lin Y, Jiang Z, Su Y, Ding X, Zhang X, et al. Enhanced optical absorption and photocatalytic activity of anatase TiO_2 through C-Nd-codoped: A DFT plus *U* calculations. J Phys Chem Solids. 2017;109:70–7.
[42] Olowoyo JO, Hernandez NC, Kumar M, Jain SL, Babalola JO, Kumar U. Insight of diversified reactivity and theoretical study of mixed-phase titanium dioxide for the photoactivation of small molecules. ChemistrySelect. 2018;3:3659–63.
[43] Sasinska A, Bialuschewski D, Islam MM, Singh T, Deo M, Mathur S. Experimental and theoretical insights into influence of hydrogen and nitrogen plasma on the water splitting performance of ALD grown TiO_2 thin films. J Phys Chem C. 2017;121(29):15538–48.
[44] Gross PA, Javahiraly N, Sabat NG, Cottineau T, Savinova ER, Keller V. Theoretical and photo-electrochemical studies of surface plasmon induced visible light absorption of Ag loaded TiO_2 nanotubes for water splitting. Appl Phys Lett. 2016;109(15):153903.
[45] Tritsaris GA, Vinichenko D, Kolesov G, Friend CM, Kaxiras E. Dynamics of the photogenerated hole at the rutile TiO_2(110)/water interface: A nonadiabatic simulation study. J Phys Chem C. 2014;118(47):27393–401.
[46] Patel M, Sanches FF, Mallia G, Harrison NM. A quantum mechanical study of water adsorption on the (110) surfaces of rutile SnO_2 and TiO_2: Investigating the effects of intermolecular interactions using hybrid-exchange density functional theory. Phys Chem Chem Phys. 2014;16(39):21002–15.
[47] Born M, Huang K, Lax M. Dynamical theory of crystal lattices. Am J Phys. 1955;39:113–27.
[48] Born M, Oppenheimer R. Zur Quantentheorie der Molekeln. Ann Der Phys. 1927;389:457–84.
[49] Makov G, Shah R, Payne MC. Periodic boundary conditions in *ab initio* calculations. II. Brillouin-zone sampling for aperiodic systems. Phys Rev B. 1996;53(23):15513–7.
[50] Hartree DR. The wave mechanics of an atom with a non-coulomb central field. Part IV. Further results relating to terms of the optical spectrum. Math Proc Camb. 1929;25:310–4.
[51] Thomas LH. The calculation of atomic fields. Math Proc Camb. 1926;21:542–6.
[52] Fermi E. Eine statistische methode zur bestimmung einiger eigenschaften des atoms und ihre anwendung auf die theorie des periodischen systems der elemente. ZS f Phys. 1928;48:73–9.
[53] Jackson K, Pederson MR. Accurate forces in a local-orbital approach to the local-density approximation. Phys Rev B. 1990;42:3276–81.
[54] Probert M. Electronic structure: Basic theory and practical methods, by Richard M. Martin. Contemp Phys. 2011;52:77.
[55] And RS, Hoffmann R. What do the Kohn-Sham orbitals and eigenvalues mean? J Am Chem Soc. 1999;121:3414–20.
[56] Tao J, Perdew JP, Staroverov VN, Scuseria GE. Climbing the density functional ladder: Nonempirical meta-generalized gradient approximation designed for molecules and solids. Phys Rev Lett. 2003;91:146401.
[57] Perdew JP, Yue W. Accurate and simple density functional for the electronic exchange energy: Generalized gradient approximation. Phys Rev B. 1986;33:8800–2.
[58] Cheng H, Selloni A. Energetics and diffusion of intrinsic surface and subsurface defects on anatase TiO_2(101). J Chem Phys. 2009;131:054703.
[59] Cohen AJ, MoriSánchez P, Yang W. Insights into current limitations of density functional theory. Science. 2008;321:792–4.
[60] Anisimov VI, Zaanen J, Andersen OK. Band theory and mott insulators: Hubbard *U* instead of stoner I. Phys Rev B. 1991;44:943–54.
[61] Finazzi E, Valentin CD, Pacchioni G, Selloni A. Excess electron states in reduced bulk anatase TiO_2: Comparison of standard GGA, GGA + *U*, and hybrid DFT calculations. J Chem Phys. 2008;129:154113.
[62] Mattioli G, Filippone F, Alippi P, Bonapasta AA. *Ab initio* study of the electronic states induced by oxygen vacancies in rutile and anatase TiO_2. Phys Rev B. 2008;78:241201.
[63] Padmanabhan KA, Basariya MR. On the common origin of structural superplasticity in different classes of materials. Rev Adv Mater Sci. 2018;54(1):1–13.
[64] Halgren TA, Lipscomb WN. The synchronous-transit method for determining reaction pathways and locating molecular transition states. Chem Phys Lett. 1977;49(2):225–32.
[65] Liang YJ, Qin HF, Huang JZ, Huan S, Hui D. Mechanical properties of boron nitride sheet with randomly distributed vacancy defects. Nanotechnol Rev. 2019;8(1):210–7.
[66] Rozhkov MA, Kolesnikova AL, Hussainova I, Kaliteevskii MA, Orlova TS, Smirnov YY, et al. Evolution of dirac cone in disclinated graphene. Rev Adv Mater Sci. 2018;57(2):137–42.
[67] Han F, Zhu L, Huang Z, Zhou Z. Photoinduced superhydrophilicity of anatase TiO_2 surface uncovered by first-principles molecular dynamics. J Phys Chem Lett. 2020;11(18):7590–4.
[68] Fan Y, Xiang Y, Shen HS. Temperature-dependent negative Poisson's ratio of monolayer graphene: Prediction from molecular dynamics simulations. Nanotechnol Rev. 2019;8(1):415–21.
[69] Zhang P, Yi WH, Xu H, Gao C, Hou J, Jin WQ, et al. Supramolecular interactions of poly[(9,9-dioctylfluorenyl-2,7-diyl)-*co*-thiophene] with single-walled carbon nanotubes. Nanotechnol Rev. 2018;7(6):487–95.
[70] Carp O, Huisman CL, Reller A. Photoinduced reactivity of titanium dioxide. Prog Solid State Ch. 2004;32(12):33–177.
[71] Park J, Lee C, Jung K, Jung D. Structure related photocatalytic properties of TiO_2. B Korean Chem Soc. 2009;30(2):402–4.
[72] Chen X, Mao SS. Titanium dioxide nanomaterials: Synthesis, properties, modifications, and applications. Chem rev. 2007;107(7):2891–959.
[73] Thompson TL, Yates JTJ. Surface science studies of the photoactivation of TiO_2–new photochemical processes. Chem Rev. 2006;106(10):4428–53.
[74] Eshaghi A, Eshaghi A. Photocatalytic properties of Cr doped TiO_2-SiO_2 nanostructure thin film. Ceram-Silikáty. 2012;56(2):135–8.
[75] Allen NS, Mahdjoub N, Vishnyakov V, Kelly PJ, Kriek RJ. The effect of crystalline phase (anatase, brookite and rutile) and

size on the photocatalytic activity of calcined polymorphic titanium dioxide (TiO_2). Polym Degrad Stabil. 2018;150:31–6.
[76] Zhou SW, Peng P, Liu J, Tang YH, Meng B, Peng YX. Investigation on the electronic structures and optical performances of Si–S codoped anatase TiO_2 by first-principles calculation. Phys Lett A. 2016;380(16):1462–8.
[77] Liu Y, Zhou W, Wu P. The electronic structure and optical properties of donor-acceptor codoped TiO_2 nanosheets from hybrid functional calculations. Mater Chem Phys. 2017;186:333–40.
[78] Ko KC, Bromley ST, Lee JY, Illas F. Size-dependent level alignment between rutile and anatase TiO_2 nanoparticles: Implications for photocatalysis. J Phys Chem Lett. 2017;8(22):5593–8.
[79] Wang Y, Feng JQ, Jin LH, Li CS. Photocatalytic reduction of graphene oxide with cuprous oxide film under UV-vis irradiation. Rev Adv Mater Sci. 2020;59(1):207–14.
[80] Rodrigues AS, Jorge MEM, Ciriaco L, Pacheco MJ, Lopes A. Perovskites (La,Ba)(Fe,Ti)O_3:AO7 photocatalysis under visible light. Rev Adv Mater Sci. 2020;59(1):151–9.
[81] Gannavarapu KP, Thakkar M, Veerapaga S, Wei LP, Dandamudi RB, Mitra S. Novel diatom-FeO_x composite as highly active catalyst in photodegradation of Rhodamine-6G. Nanotechnol Rev. 2018;7(3):247–55.
[82] Guo Q, Zhou C, Ma Z, Yang X. Fundamentals of TiO_2 photocatalysis: Concepts, mechanisms, and challenges. Adv Mater. 2019;31(50):1901997.
[83] Tang J, Durrant JR, Klug DR. Mechanism of photocatalytic water splitting in TiO(2). Reaction of water with photoholes, importance of charge carrier dynamics, and evidence for four-hole chemistry. J Am Chem Soc. 2008;130(42):13885–91.
[84] Valdes A, Qu ZW, Kroes GJ, Rossmeisl J, Norskov JK. Oxidation and photo-oxidation of water on TiO_2 surface. J Phys Chem C. 2008;112(26):9872–9.
[85] Salvador P, Gutierrez C. The nature of surface states involved in the photo- and electroluminescence spectra of n-titanium dioxide electrodes. J Phys Chem. 1984;88(16):3696–8.
[86] Norton AP, Bernasek SL, Bocarsly AB. Mechanistic aspects of the photooxidation of water at the *n*-titania/aqueous interface: Optically induced transients as a kinetic probe. J Phys Chem. 1988;92(21):6009–16.
[87] Salvador P. On the nature of photogenerated radical species active in the oxidative degradation of dissolved pollutants with TiO_2 aqueous suspensions: A revision in the light of the electronic structure of adsorbed water. J Phys Chem C. 2007;111(45):17038–43.
[88] Salvador P. Mechanisms of water photooxidation at n-TiO_2 rutile single crystal oriented electrodes under UV illumination in competition with photocorrosion. Prog Surf Sci. 2011;86(1–2):41–58.
[89] Zhao W, Liu Z. Mechanism and active site of photocatalytic water splitting on titania in aqueous surroundings. Chem Sci. 2014;5(6):2256–64.
[90] Imanishi A, Okamura T, Ohashi N, Nakamura R, Nakato Y. Mechanism of water photooxidation reaction at atomically flat TiO_2 (rutile) (110) and (100) surfaces: Dependence on solution pH. J Am Chem Soc. 2007;129(37):11569–78.
[91] Shao Y, de Groot HJM, Buda F. Proton acceptor near the active site lowers dramatically the O–O bond formation energy barrier in photocatalytic water splitting. J Phys Chem Lett. 2019;10(24):7690–7.
[92] Kumaravel V, Mathew S, Bartlett J, Pillai SC. Photocatalytic hydrogen production using metal doped TiO_2: A review of recent advances. Appl Catal B-Environ. 2019;244:1021–64.
[93] Jaihindh DP, Verma A, Chen C, Huang Y. Study of oxidation states of Fe- and Co-doped TiO_2 photocatalytic energy materials and their visible-light-driven photocatalytic behavior. Int J Hydrog Energ. 2019;44(30):15892–906.
[94] Kato M, Najima H, Ozawa T. Effects of Nb doping on the photocatalytic performance of rutile TiO_2 single crystals. J Electrochem Soc. 2019;166(10):H468–72.
[95] Zhuk NA, Belyy VA, Lutoev VP, Makeev BA, Nekipelov SV, Sivkov VN, et al. Phase transition of $BiNb_{1-x}Mn_xO_4$–delta: Thermal analyse, NEXAFS, XPS and ESR-study. Rev Adv Mater Sci. 2019;58(1):171–8.
[96] Asahi R, Morikawa T, Ohwaki T, Aoki K, Taga Y. Visible-light photocatalysis in nitrogen-doped titanium oxides. Science. 2001;293(5528):269–71.
[97] Enriquez JIG, Moreno JLV, David MY, Arboleda NB, Lin OH, Villagracia AC. DFT investigation on the electronic and water adsorption properties of pristine and N-Doped TiO_2 nanotubes for photocatalytic water splitting applications. J Elrctron Mater. 2017;46(6):3592–602.
[98] Taherinia M, Nasiri M, Abedini E, Pouretedal HR. Comparing the photocatalytic activity of N-doped and S-doped titanium dioxide nanoparticles for water splitting under sunlight radiation. J Iran Chem Soc. 2018;15(6):1301–10.
[99] Tian F, Liu C. DFT description on electronic structure and optical absorption properties of anionic S-doped anatase TiO_2. J Phys Chem B. 2006;110(36):17866–71.
[100] Peng Y, He J, Liu Q, Sun Z, Yan W, Pan Z, et al. Impurity concentration dependence of optical absorption for phosphorus-doped anatase TiO_2. J Phys Chem C. 2011;115(16):8184–8.
[101] Wu H, Lin S, Wu J. Effects of nitrogen concentration on N-doped anatase TiO_2: Density functional theory and Hubbard *U* analysis. J Alloy Compd. 2012;522:46–50.
[102] Beloseviccavor J, Koteski V, Umicevic A, Ivanovski V. Effect of 5d transition metals doping on the photocatalytic properties of rutile TiO_2. Comp Mater Sci. 2018;151:328–37.
[103] Su Q, Han Q, Gao J, Wen H, Jiang Z. Modification of the photocatalytic properties of anatase TiO_2(101) surface by doping transition metals. ACTA Phys Sin. 2017;66(6):067101.
[104] Basavarajappa PS, Patil SB, Ganganagappa N, Reddy KR, Raghu AV, Reddy CV. Recent progress in metal-doped TiO_2, non-metal doped/codoped TiO_2 and TiO_2 nanostructured hybrids for enhanced photocatalysis. Int J Hydrog Energ. 2020;45(13):7764–78.
[105] Wang S, Bai LN, Sun H, Jiang Q, Lian J. Structure and photocatalytic property of Mo-doped TiO_2 nanoparticles. Powder Technol. 2013;244:9–15.
[106] Karvinen S, Hirva P, Pakkanen TA. *Ab initio* quantum chemical studies of cluster models for doped anatase and rutile TiO_2. J Mol Struc-Theochem. 2003;626(1):271–7.
[107] Chiodi M, Cheney CP, Vilmercati P, Cavaliere E, Mannella N, Weitering HH, et al. Enhanced dopant solubility and visible-light absorption in Cr-N codoped TiO_2 nanoclusters. J Phys Chem C. 2012;116(1):311–8.

[108] Cheney CP, Vilmercati P, Martin EW, Chiodi M, Gavioli L, Regmi M, et al. Origins of electronic band gap reduction in Cr/N codoped TiO_2. Phys Rev Lett. 2014;112(3):036404.
[109] Kim W, Tachikawa T, Kim H, Lakshminarasimhan N, Murugan P, Park H, et al. Visible light photocatalytic activities of nitrogen and platinum-doped TiO_2: Synergistic effects of co-dopants. Appl Catal B-Environ. 2014;147:642–50.
[110] Sun X, Liu H, Dong J, Wei J, Zhang Y. Preparation and characterization of Ce/N-codoped TiO_2 particles for production of H_2 by photocatalytic splitting water under visible light. Catal Lett. 2010;135(3):219–25.
[111] Yang L, Gao P, Lu J, Guo W, Zhuang Z, Wang Q, et al. Mechanism analysis of Au, Ru noble metal clusters modified on TiO_2(101) to intensify overall photocatalytic water splitting. RSC Adv. 2020;10(35):20654–64.
[112] Zhao H, Cui S, Yang L, Li G, Li N, Li X. Synthesis of hierarchically meso-macroporous TiO_2/CdS heterojunction photocatalysts with excellent visible-light photocatalytic activity. J Colloid Interf Sci. 2018;17:47–54.
[113] Liao Y, Deng P, Wang X, Zhang D, Li F, Yang Q, et al. A facile method for preparation of Cu_2O-TiO_2 NTA heterojunction with visible-photocatalytic activity. Nanoscale Res Lett. 2018;13:221.
[114] Sha MA, Meenu PC, Sumi VS, Bhagya TC, Sreelekshmy BR, Shibli SMA. Tuning of electron transfer by Ni–P decoration on CeO_2–TiO_2 heterojunction for enhancement in photocatalytic hydrogen generation. Mat Sci Semicon Proc. 2020;105:104742.
[115] Kumar S, Sharma S, Sood S, Umar A, Kansal SK. Bismuth sulfide (Bi_2S_3) nanotubes decorated TiO_2 nanoparticles heterojunction assembly for enhanced solar light driven photocatalytic activity. Ceram Int. 2016;42(15):17551–7.
[116] Li Y, Zhang P, Wan D, Xue C, Zhao J, Shao G. Direct evidence of 2D/1D heterojunction enhancement on photocatalytic activity through assembling MoS_2 nanosheets onto super-long TiO_2 nanofibers. Appl Surf Sci. 2020;504:144361.
[117] Li J, Zhang M, Li X, Li Q, Yang J. Effect of the calcination temperature on the visible light photocatalytic activity of direct contact Z-scheme g-C_3N_4-TiO_2 heterojunction. Appl Catal B-Environ. 2017;212:106–14.
[118] Xu Q, Zhang L, Yu J, Wageh S, Al-Ghamdi AA, Jaroniec M. Direct Z-scheme photocatalysts: Principles, synthesis, and applications. Mater Today. 2018;21(10):1042–63.
[119] Wang J, Wang G, Wang X, Wu Y, Su Y, Tang H. 3D/2D direct Z-scheme heterojunctions of hierarchical TiO_2 microflowers/g-C_3N_4 nanosheets with enhanced charge carrier separation for photocatalytic H-2 evolution. Carbon. 2019;149:618–26.
[120] Yun HJ, Lee H, Kim ND, Lee DM, Yu S, Yi J. A combination of two visible-light responsive photocatalysts for achieving the Z-scheme in the solid state. ACS Nano. 2011;5(5):4084–90.
[121] Xiao LM, Liu TF, Zhang M, Li QY, Yang JJ. Interfacial construction of zero-dimensional/one-dimensional g-C_3N_4 nanoparticles/TiO_2 nanotube arrays with Z-scheme heterostructure for improved photoelectrochemical water splitting. ACS Sustain Chem Eng. 2019;7(2):2483–91.
[122] Wang H, Hu Z, Li H. Dissociation of liquid water on defective rutile TiO_2(110) surfaces using *ab initio* molecular dynamics simulations. Front Phys. 2018;13(3):138107.
[123] Zhou G, Liu C, Huang L. Molecular dynamics simulation of first-adsorbed water layer at titanium dioxide surfaces. J Chem Eng Data. 2018;63(7):2420–9.
[124] Kowalski PM, Meyer B, Marx D. Composition, structure, and stability of the rutile TiO_2(110) surface: Oxygen depletion, hydroxylation, hydrogen migration, and water adsorption. Phys Rev B. 2009;79:115410.
[125] Ma X, Wu X, Zhao X, Sun H. Geometric and electronic properties of ultrathin anatase TiO_2(001) films. Phys Chem Chem Phys. 2017;19(37):25456–62.
[126] Zhao Z. Single water molecule adsorption and decomposition on the low-index stoichiometric rutile TiO_2 surfaces. J Phys Chem C. 2014;118(8):4287–95.
[127] Kim CW, Yeob SJ, Cheng H, Kang YS. A selectively exposed crystal facet-engineered TiO_2 thin film photoanode for the higher performance of the photoelectrochemical water splitting reaction. Energ Env Sci. 2015;8(12):3646–53.
[128] Guo Q, Minton TK, Yang X. Elementary processes in photo catalysis of methanol and water on rutile TiO_2(110): A new picture of photocatalysis. Chin J Catal. 2015;36(10):1649–55.
[129] Ji Y, Wang B, Luo Y. GGA + *U* study on the mechanism of photodecomposition of water adsorbed on rutile TiO_2(110) surface: Free vs trapped hole. J Phys Chem C. 2014;118:1027–34.
[130] Harris LA, Quong AA. Molecular chemisorption as the theoretically preferred pathway for water adsorption on ideal rutile TiO_2(110). Phys Rev Lett. 2004;93:086105.
[131] Kumar N, Kent PRC, Wesolowski DJ, Kubicki JD. Modeling water adsorption on rutile (110) using van der Waals density functional and DFT + *U* methods. J Phys Chem C. 2013;117:23638–44.
[132] Wesolowski DJ, Sofo JO, Bandura AV, Zhang Z, Mamontov E, Předota M, et al. Comment on "structure and dynamics of liquid water on rutile TiO_2(110)". Phys Rev B. 2012;85:167401.
[133] Patrick CE, Giustino F. Structure of a water monolayer on the anatase TiO_2(101) surface. Phys Rev Appl. 2014;2(1):014001.
[134] Migani A, Mowbray DJ, Zhao J, Petek H. Quasiparticle interfacial level alignment of highly hybridized frontier levels: H_2O on TiO_2(110). J Chem Theory Comput. 2015;11:239–51.
[135] Brandt EG, Lyubartsev AP. Systematic optimization of a force field for classical simulations of TiO_2–water interfaces. J Phys Chem C. 2015;119(32):18110–25.
[136] Kavathekar RS, Dev P, English NJ, MacElroy JMD. Molecular dynamics study of water in contact with the TiO_2 rutile-110, 100, 101, 001 and anatase-101, 001 surface. Mol Phys. 2011;109(13):1649–56.
[137] Sun C, Liu L, Selloni A, Lu G, Smith SC. Titania-water interactions: A review of theoretical studies. J Mater Chem. 2010;20(46):10319–34.
[138] Ohler B, Langel W. Molecular dynamics simulations on the interface between titanium dioxide and water droplets: A new model for the contact angle. J Phys Chem C. 2009;113(23):10189–97.
[139] Vlcek L, Cummings PT. Adsorption of water on TiO_2 and SnO_2 surfaces: Molecular dynamics study. Collect Czech Chem C. 2008;73(4):575–89.
[140] Předota M, Bandura AV, Cummings PT, Kubicki JD, Wesolowski DJ, Chialvo AA, et al. Electric double layer at the rutile (110) surface. 1. Structure of surfaces and interfacial water from molecular dynamics by use of *ab initio* potentials. J Phys Chem B. 2004;108(32):12049–60.
[141] Friedrichs W, Langel W. Atomistic modeling of peptide adsorption on rutile (100) in the presence of water and of

contamination by low molecular weight alcohols. Biointerphases. 2014;9(3):031006.
[142] Dohn AO, Selli D, Fazio G, Ferraro L, Mortensen JJ, Civalleri B, et al. Interfacing CRYSTAL/AMBER to Optimize QM/MM Lennard–Jones parameters for water and to study solvation of TiO_2 nanoparticles. Molecules. 2018;23(11):2958–81.
[143] Mamontov E, Vlcek L, Wesolowski DJ, Cummings PT, Wang W, Anovitz LM, et al. Dynamics and structure of hydration water on rutile and cassiterite nanopowders studied by quasi-elastic neutron scattering and molecular dynamics simulations. J Phys Chem C. 2007;111(11):4328–41.
[144] Kim S, Kumar N, Persson P, Sofo J, van Duin ACT, Kubicki JD. Development of a ReaxFF reactive force field for titanium dioxide/water systems. Langmuir. 2013;29(25):7838–46.
[145] Bahramian A. Molecular interactions insights underlying temperature-dependent structure of water molecules on TiO_2 nanostructured film: A computational study using reactive and non-reactive force fields. Fluid Phase Equilibr. 2017;438:53–66.
[146] Huang L, Gubbins KE, Li L, Lu X. Water on titanium dioxide surface:a revisiting by reactive molecular dynamics simulations. Langmuir. 2014;30(49):14832–40.
[147] Futera Z, English NJ. Exploring rutile (110) and anatase (101) TiO_2 water interfaces by reactive force-field simulations. J Phys Chem C. 2017;121(12):6701–11.
[148] Sheng H, Zhang H, Song W, Ji H, Ma W, Chen C, et al. Activation of water in titanium dioxide photocatalysis by formation of surface hydrogen bonds: An *in situ* IR spectroscopy study. Angew Chem Int Ed. 2015;54(20):5905–9.
[149] Margineda J, English NJ. Dynamical and structural properties of adsorbed water molecules at the TiO_2 anatase-(1 0 1) surface: Importance of interfacial hydrogen-bond rearrangements. Chem Phys Lett. 2020;743:137164.
[150] Kumar N, Neogi S, Kent PR, Bandura AV, Kubicki JD, Wesolowski DJ, et al. Hydrogen bonds and vibrations of water on (110) rutile. J Phys Chem C. 2009;113(31):13732–40.
[151] English NJ. Dynamical properties of physically adsorbed water molecules at the TiO_2 rutile-(110) surface. Chem Phys Lett. 2013;583:125–30.
[152] Mattioli G, Filippone F, Caminiti R, Bonapasta AA. Short hydrogen bonds at the water/TiO_2 (anatase) interface. J Phys Chem C. 2008;112(35):13579–86.
[153] English NJ, Kavathekar RS, MacElroy JMD. Hydrogen bond dynamical properties of adsorbed liquid water monolayers with various TiO_2 interfaces. Mol Phys. 2012;110(23):2919–25.
[154] Nakamura R, Nakato Y. Primary intermediates of oxygen photoevolution reaction on TiO_2 (Rutile) particles, revealed by *in situ* FTIR absorption and photoluminescence measurements. J Am Chem Soc. 2004;126(4):1290–8.
[155] Nakamura R, Okamura T, Ohashi N, Imanishi A, Nakato Y. Molecular mechanisms of photoinduced oxygen evolution, PL emission, and surface roughening at atomically smooth (110) and (100) *n*-TiO_2 (Rutile) surfaces in aqueous acidic solutions. J Am Chem Soc. 2005;127(37):12975–83.
[156] Rossmeisl J, Qu ZW, Zhu H, Kroes GJ, Nørskov JK. Electrolysis of water on oxide surfaces. Electroanal Chem. 2007;607(1):83–9.
[157] Nozik A. Photoelectrolysis of water using semiconducting TiO_2 crystals. Nature. 1975;257:383–6.
[158] Wang D, Sheng T, Chen J, Wang H, Hu P. Identifying the key obstacle in photocatalytic oxygen evolution on rutile TiO_2. Nat Catal. 2018;1(4):291–9.
[159] Jin F, Wei M, Chen T, Ma H, Liu G, Ma Y. Behavior of photogenerated electron–hole pair for water splitting on TiO_2(110). J Phys Chem C. 2018;122(40):22930–8.
[160] Kim N, Turner E, Kim Y, Ida S, Hagiwara H, Ishihara T, et al. Two-dimensional TiO_2 nanosheets for photo and electrochemical oxidation of water: Predictions of optimal dopant species from first-principles. J Phys Chem C. 2017;121(35):19201–8.
[161] Lang X, Liang YH, Zhang J, Li L, Cao L, Zhang H. Structure and reactivity of a water-covered anatase TiO_2(001) surface. Phys Chem Chem Phys. 2020;22(3):1371–80.
[162] Li Y, Liu Z, Liu L, Gao W. Mechanism and activity of photocatalytic oxygen evolution on titania anatase in aqueous surroundings. J Am Chem Soc. 2010;132(37):13008–15.
[163] Valdes A, Qu ZW, Kroes GJ. Oxidation and photo-oxidation of water on TiO_2 surface. J Phys Chem C. 2008;112(26):9872–9.
[164] Chen J, Li Y, Sit PH, Selloni A. Chemical dynamics of the first proton-coupled electron transfer of water oxidation on TiO_2 anatase. J Am Chem Soc. 2013;135(50):18774–7.
[165] Siahrostami S, Vojvodic A. Influence of adsorbed water on the oxygen evolution reaction on oxides. J Phys Chem C. 2015;119(2):1032–7.
[166] Ariyanti D, Mukhtar S, Ahmed N, Liu Z, Dong J, Gao W. Surface modification of TiO_2 for visible light photocatalysis: Experimental and theoretical calculations of its electronic and optical properties. Int J Mod Phys B. 2020;33:2040067.
[167] Kohtani S, Kawashima A, Miyabe H. Reactivity of trapped and accumulated electrons in titanium dioxide photocatalysis. Catalysts. 2017;7(10):7100303.
[168] Selcuk S, Selloni A. Excess electrons at anatase TiO_2 surfaces and interfaces: Insights from first principles simulations. J Phys D Appl Phys. 2017;50(27):273002.
[169] Morita K, Yasuoka K. Density functional theory study of atomic and electronic properties of defects in reduced anatase TiO_2 nanocrystals. AIP Adv. 2018;8(3):5021024.
[170] Ji Y, Wang B, Luo Y. Location of trapped hole on rutile-TiO_2(110) surface and its role in water oxidation. J Phys Chem C. 2012;116(14):7863–6.
[171] Cheng J, Vandevondele J, Sprik M. Identifying trapped electronic holes at the aqueous TiO_2 interface. J Phys Chem C. 2014;118(10):5437–44.
[172] Jedidi A, Markovits A, Minot C, Bouzriba S, Abderraba M. Modeling localized photoinduced electrons in rutile-TiO_2 using periodic DFT + *U* methodology. Langmuir. 2010;26(21):16232–8.
[173] Koitaya T, Nakamura H, Yamashita K. First-principle calculations of solvated electrons at protic solvent-TiO_2 interfaces with oxygen vacancies. J Phys Chem C. 2009;113(17):7236–45.
[174] Fischer SA, Duncan WR, Prezhdo OV. *Ab initio* nonadiabatic molecular dynamics of wet-electrons on the TiO_2 surface. J Am Chem Soc. 2009;131(42):15483–91.
[175] Onda K, Li B, Zhao J, Jordan KD, Yang J, Petek H. Wet electrons at the H_2O/TiO_2(110) surface. Science. 2005;308(5725):1154–8.

[176] Zhang H, Zhu Y, Zhao M. Interface charge transfer and enhanced visible light response of graphene/anatase TiO_2(110) systems with and without oxygen vacancy: A DFT plus *U* calculation. Appl Surf Sci. 2017;420:105–9.
[177] Reilly K, Wilkinson DP, Taghipour F. Photocatalytic water splitting in a fluidized bed system: Computational modeling and experimental studies. Appl Energ. 2018;222: 423–36.
[178] Hu J, Xie J, Jia W, Zhang S, Wang S, Wang K, et al. Interesting molecule adsorption strategy induced energy band tuning: Boosts 43 times photocatalytic water splitting ability for commercial TiO_2. Appl Catal B-Environ. 2020;268: 118753.
[179] Mehdipour H, Akimov AV, Jankowska J, Rezakhanai AT, Tafreshi SS, de Leeuw NH, et al. Persistent quantum coherence and strong coupling enable fast electron transfer across the CdS/TiO_2 interface: A time-domain *ab initio* simulation. J Phys Chem C. 2018;122(44):25606–16.
[180] Wei Y, Zhou Z, Fang W, Long R. Grain boundary facilitates photocatalytic reaction in rutile TiO_2 despite fast charge recombination: A time-domain *ab initio* analysis. J Phys Chem Lett. 2018;9(19):5884–9.
[181] Lu T, Wang Y, Tomko JA, Hopkins PE, Zhang H, Prezhdo OV. Control of charge carrier dynamics in plasmonic Au films by TiO_x substrate stoichiometry. J Phys Chem Lett. 2020;11(4):1419–27.
[182] Nam Y, Li L, Lee JY, Prezhdo OV. Size and shape effects on charge recombination dynamics of TiO_2 nanoclusters. J Phys Chem C. 2018;122(9):5201–8.
[183] Wei Y, Li L, Fang W, Long R, Prezhdo OV. Weak Donor–Acceptor interaction and interface polarization define photoexcitation dynamics in the MoS_2/TiO_2 composite: Time-domain *ab initio* simulation. Nano Lett. 2017;17(7):4038–46.
[184] Muuronen M, Parker SM, Berardo E, Le A, Zwijnenburg MA, Furche F. Mechanism of photocatalytic water oxidation on small TiO_2 nanoparticles. Chem Sci. 2017;8(3):2179–83.
[185] Long R, Fang W, Prezhdo OV. Strong interaction at the perovskite/TiO_2 interface facilitates ultrafast photoinduced charge separation: A nonadiabatic molecular dynamics study. J Phys Chem C. 2017;121(7):3797–806.